A MULTISCALE HYBRID METHOD*

GABRIEL R. BARRENECHEA †, ANTONIO TADEU A. GOMES ‡, AND DIEGO PAREDES §

Abstract. In this work we propose, analyze, and test a new multiscale finite element method called Multiscale Hybrid (MH) method. The method is built as a close relative to the Multiscale Hybrid Mixed (MHM) method, but with the fundamental difference that a novel definition of the Lagrange multiplier is introduced. The practical implication of this is that both the local problems to compute the basis functions, as well as the global problem, are elliptic, as opposed to the MHM method (and also other previous methods) where a mixed global problem is solved, and constrained local problems are solved to compute the local basis functions. The error analysis of the method is based on a hybrid formulation, and a static condensation process is done at the discrete level, so the final global system only involves the Lagrange multipliers. We tested the performance of the method by means of numerical experiments for problems with multiscale coefficients, and we carried out comparisons with the MHM method in terms of performance, accuracy, and memory requirements.

Key words. Multiscale finite element; hybrid problem; multiscale diffusion equation.

MSC codes. 65N30; 65M12; 65Y20.

1. Introduction. The field of numerical analysis, specifically in addressing multiscale problems through finite element methods, has seen considerable growth since the foundational work by Babuška and Osborn [6]. This area has branched into various innovative methods like the Variational Multiscale Method (VMS) [27], Multiscale Finite Element Method (MsFEM), its generalization (GMsFEM) [16], Heterogeneous Multiscale Method (HMM) [14], Multiscale Mortar Method [5], Local Orthogonal Decomposition (LOD) Method [29, 30], Hybrid Localized Spectral Decomposition (LSD) method [32], and the Higher Order hybrid Multiscale Method (MsHHO) [13]. These developments, along with enriched methods that are closely related to multiscale approaches, demonstrate the field's diversity and evolution, as detailed in numerous comprehensive surveys and studies [16, 4, 29, 15, 31, 1]. One particular example of such a method, developed in the last decade, is the Multiscale Hybrid Method (MHM), originally proposed in [25, 3] for multiscale problems in porous media, and further developed for different partial differential equations (see, e.g., [26, 12] for its application for different models, and [8, 20] for its extension to polytopic meshes). The starting point of the MHM method is the proposal of a hybrid formulation for the partial differential equation at hand. Then, static condensation is performed at the continuous level leading to a problem with two unknowns, namely, the Lagrange multipliers in the inter-element facets, and one unknown per element that belongs to a local kernel (piecewise constants in the case of scalar problems [3], rigid modes in the case of linear elasticity [24]). As such, the resulting system is a *mixed* problem. The reason for the mixed character of the problem can be explained as follows: the

*Submitted to the editors on 12/21/2022.

Funding: The work of GRB has been partially funded by the Leverhulme Trust through the Research Project Grant No. RPG-2021-238. DP was partially supported by Project EOLIS (MATH-AMSUD 21-MATH-04) and ANID-Chile through Grant FONDECYT-1181572.

†Dept. of Mathematics and Statistics, University of Strathclyde, 26 Richmond Street, Glasgow G1 1XH, UK (gabriel.barrenechea@strath.ac.uk).

‡Dept. of Mathematical and Computational Methods, National Laboratory for Scientific Computing (LNCC), Av. Getulio Vargas 333, Petropolis RJ, Brazil (atagomes@lncc.br).

§Departamento de Ingeniería Matemática and CI^{2}MA, Universidad de Concepción, Chile (dparedes@udec.cl).

Lagrange multipliers are the normal fluxes, that is, the normal derivative of the primal unknown in the case of the Poisson equation. So, the local problems defining the basis functions include Neumann conditions, and thus to get a well-posed problem the solution needs to be sought in the space of functions with zero mean value in each element. One alternative view, linking the MHM method to the solution of an elliptic problem, was taken in the recent work [10]. It is proven in that work under certain hypotheses (e.g., that the second level problems are solved in an exact way) that the discrete solution of the MHM method coincides with that of the MsHHO method. The MsHHO is driven by an elliptic global problem (with local mixed problems), so [10] opens the door to more insights into the stability of the MHM method, along with a unified error analysis for the primal variable.

The issue of local problems with Neumann boundary conditions has been encountered in several different contexts, probably the most noticeable being domain decomposition methods. In fact, this is one of the main reasons behind the use of Robin boundary conditions in the Optimized Schwarz Method (OSM) proposed as far back as [28]. Since then, several different proposals to use Robin boundary conditions have been used to remove local singularities. For example, and just restricting ourselves to the context of recent multiscale finite element methods, in [22] the Multiscale Robin Coupled Method (MRCM) starts from a mixed problem in porous media, and generates basis functions that are solutions of local problems containing Robin boundary conditions; both the local and the global problems are written in mixed form, and comparisons are drawn (see also [23, 38] for the application of the same idea to different models, mostly linked to flow through porous media). Also, in [34] the multiscale Latin method is analyzed, and the optimal choice of the Robin parameter is studied. This last point is a common thread in the domain decomposition community. In fact, looking for optimal Robin parameters has been the topic of several works in domain decomposition, see [19] as an example.

The purpose of this work is to build up on the idea of using Robin boundary conditions on the local problems to propose a new Multiscale Hybrid (MH) finite element method. After partitioning the domain into elements (of general shape) a new hybrid formulation is proposed. In it, the Lagrange multiplier (denoted λ) is not equal to the normal flux (as in standard hybrid methods), but it is perturbed by adding a term that depends on the primal variable (denoted u). This process presents the advantage that the bilinear form in the bulk is elliptic in the whole broken space (thus removing the kernel that would have arisen otherwise), and that its well-posedness can be analyzed using standard arguments for variational problems with constraints. We then discretize this hybrid problem using discontinuous approximations for λ, and globally discontinuous (but continuous in each polyhedral element) finite element spaces for u. Due to the particular structure of the new formulation, error estimates that are independent of the Robin parameter can be proven.

The final step in the building of the method is the static condensation process. For this, the discontinuous character of the approximation space for u is exploited to write its degrees of freedom in terms of those for λ. This is where the fact that the bilinear form in the bulk is not only elliptic in the discrete kernel, but in fact *elliptic in the whole broken space, and locally in each element of the partition*, can be fully exploited. In fact, this leads to two main advantages of this method: first, the local problems are well-posed in the whole local space (without any extra constraints); in addition, and as a consequence of this, the global problem is driven by an elliptic bilinear form involving only the unknowns for the Lagrange multiplier (thus avoiding the solution of a mixed problem). To keep the presentation simple, we have focused

in this work to the diffusion equation with multiscale coefficients, but the strategy proposed herein can be extended naturally to more complex situations.

The rest of the paper is organized as follows. We finish this introduction by presenting the model problem and the main notations, assumptions, and preliminary results used in the rest of the manuscript. In section 2 we present the new hybrid formulation, and prove its well-posedness and equivalence with the original primal weak form. We also present its discrete counterpart, and prove stability and optimal-order error estimates, the latter under appropriate regularity assumptions on the exact solution and coefficients. The MH method is then introduced in section 3 as a result of a static condensation procedure. We detail the rewriting of the hybrid problem as one whose only unknowns are the discrete Lagrange multipliers, and prove its ellipticity. In addition, we present a short section on the implementation and main features of the computational algorithm. The performance of the method, and comparisons with previously existing methods, are presented in section 4 using four series of numerical experiments. Finally, we outline some conclusions and open questions.

1.1. The model problem. Let $\Omega \subset \mathbb{R}^d$, $d \in \{2, 3\}$, be an open, bounded, polygonal, domain with Lipschitz boundary $\partial\Omega$. We consider the problem of finding $u : \Omega \to \mathbb{R}$ such that:

$$\left\{ \begin{array}{rcll} \operatorname{div}(-\mathcal{K}\nabla u) & = & f\,, & \text{in } \Omega \\ u & = & 0\,, & \text{on } \partial\Omega \end{array} \right. , \tag{1.1}$$

where $f \in L^2(\Omega)$ is a given datum and the diffusive coefficient $\mathcal{K} = (\mathcal{K}_{ij})_{i,j=1}^d \in L^\infty(\Omega)^{d\times d}$ is a symmetric tensor supposed to be uniformly elliptic, i.e., there exist positive constants $\mathcal{K}_{\min}$ and $\mathcal{K}_{\max}$, such that

$$\mathcal{K}_{\min}\,|\boldsymbol{\xi}|^2 \le \mathcal{K}_{ij}(\boldsymbol{x})\xi_i\xi_j \le \mathcal{K}_{\max}\,|\boldsymbol{\xi}|^2 \quad \text{for all } \boldsymbol{\xi} = \{\xi_i\} \in \mathbb{R}^d, \text{ and almost all } \boldsymbol{x} \in \bar{\Omega}\,. \tag{1.2}$$

The functions f and $\mathcal{K}$ may involve multi-scale features. For the derivation of the method and its stability analysis it is enough to assume that the diffusion coefficient belongs only to $L^\infty(\Omega)^{d\times d}$. In addition, in our numerical experiments we have approximated a partial differential equation with rough coefficients. Nevertheless, the error analysis of the method relies in an implicit regularity requirement for the coefficient $\mathcal{K}$, which will be made explicit later.

1.2. Partitions and triangulations. Following closely the definitions initially proposed in [8], we introduce two partitions which do not necessarily coincide but are not independent. To avoid technical diversions, we will restrict the presentation, and all the proofs, to the two-dimensional situation. Nevertheless, the results presented below can be extended to the three-dimensional case by proceeding as in [20]. First, we introduce a family $\{\mathscr{P}_\mathcal{H}\}_{\mathcal{H}>0}$, of partitions of $\bar{\Omega}$, composed by closed, bounded, disjoint polygons. (We make more precise hypotheses on the polygons later on.) The diameter of a polygonal element $K \in \mathscr{P}_\mathcal{H}$ is denoted by $\mathcal{H}_K$, and the radius of its inscribed circle is denoted by ρ_K. We set $\mathcal{H} := \max_{K\in\mathscr{P}_\mathcal{H}} \mathcal{H}_K$ and assume the existence of $c > 0$ such that

$$\frac{\mathcal{H}_K}{\rho_K} \le c, \text{ for all } K \in \mathscr{P}_\mathcal{H}, \text{ for all } \mathcal{H} > 0. \tag{1.3}$$

Each polygon K has a boundary ∂K consisting of edges E. The set of boundaries of the elements in $\mathscr{P}_\mathcal{H}$ is denoted by $\partial\mathscr{P}_\mathcal{H}$ and the set of its edges by $\mathcal{E}$; that is

$\partial\mathscr{P}_\mathcal{H} = \{\partial K : K \in \mathscr{P}_\mathcal{H}\}$, and,

$$\mathcal{E} = \left\{ \begin{array}{c} E = \partial K \cap \partial K', \text{ or} \\ E = \partial K \cap \partial\Omega \end{array} \middle| \begin{array}{c} K, K' \in \mathscr{P}_\mathcal{H}, K \neq K', \text{ and} \\ E \text{ is not a single point} \end{array} \right\}.$$

To each $E \in \mathcal{E}$ we associate a normal $\boldsymbol{n}^E$; its orientation is not important, but is fixed. For each $K \in \mathscr{P}_\mathcal{H}$ we further denote by $\boldsymbol{n}^K$ the outward normal vector on ∂K, and let $\boldsymbol{n}_E^K := \boldsymbol{n}^K|_E$ for each $E \subset \partial K$. The first step toward defining a computational mesh is to introduce $\mathcal{E}_H$, a partition of the facets in $\mathcal{E}$ into segments F of length $H_F \leq H := \max_{F\in\mathcal{E}_H} H_F$, and such that each $F \in \mathcal{E}_H$ is a subset of only one $E \in \mathcal{E}$. We will not assume that the segments are of equal length, but we will require that they are not too different. More precisely, we impose the following Assumption.

Assumption (A1) The mesh $\mathcal{E}_H$ is such that in every $K \in \mathscr{P}_\mathcal{H}$ a shape-regular simplicial triangulation $\Xi_H(K)$ of K can be built such that its trace on ∂K coincides with $\mathcal{E}_H$.

The last ingredient in the definition of the discrete scheme is the mesh that will be used to approximate the local basis functions: for each $K \in \mathscr{P}_\mathcal{H}$, we introduce a shape regular family of simplicial triangulations $\{\mathscr{T}_h^K\}_{h>0}$ built in the following way:

1. first, on each $K \in \mathscr{P}$, the triangulation $\Xi_H(K)$ is refined once using a *red refinement* [7]. The resulting triangulation is called *minimal triangulation*;
2. then, for each K, the family $\{\mathscr{T}_h^K\}_{h>0}$ is formed by regular refinements of the minimal triangulation.

The diameter of $\mathfrak{T} \in \mathscr{T}_h^K$ is denoted by $h_\mathfrak{T}$, and $h := \max_{K\in\mathscr{P}_\mathcal{H}} \max_{\mathfrak{T}\in\mathscr{T}_h^K} h_\mathfrak{T}$, and $\mathscr{T}_h := \cup_{K\in\mathscr{P}_\mathcal{H}} \mathscr{T}_h^K$. It is important to remark that, if $E = K \cap K' \in \mathcal{E}$, then the traces of the two neighbouring triangulations $\mathscr{T}_h^K$ and $\mathscr{T}_h^{K'}$ do not necessarily coincide. In Figure 1 we show one example of partitions that satisfy the above assumptions.

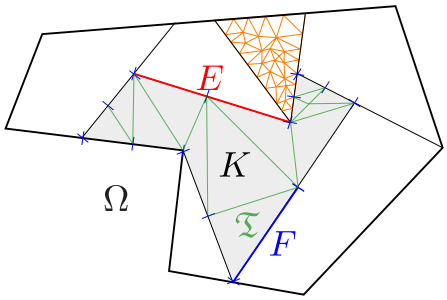

FIG. 1. *A domain Ω partitioned by $\mathscr{P}_\mathcal{H}$ with non-conforming polygonal elements. Observe the sub-meshes (green and orange) discretizing two different elements of $\mathscr{P}_\mathcal{H}$ with different granularity, where $\mathfrak{T} \in \mathscr{T}_h^K$ is an element of the discretization of $K \in \mathscr{P}_\mathcal{H}$. The red line represents an edge $E \in \mathcal{E}$ and the blue line represents an element $F \in \mathcal{E}_H$ of the skeleton mesh.*

1.3. Spaces, inner products, and norms. We follow the standard notation for Lebesgue and Sobolev spaces, in line with, e.g., [17]. For $K \in \mathscr{P}_\mathcal{H}$ and $m \geq 1$, we consider the local space $H^m(K)$ equipped with the semi-norm $|\cdot|_{m,K}$ and the norm $\|\cdot\|_{m,K}$, with their usual definitions. We then define the broken space

$$H^m(\mathscr{P}_\mathcal{H}) := \{v \in L^2(\Omega) : v|_K \in H^m(K) \text{ for all } K \in \mathscr{P}_\mathcal{H}\}, \tag{1.4}$$

equipped with the semi-norm and norm,

$$|v|_{m,\mathscr{P}_{\mathcal{H}}} := \left(\sum_{K\in\mathscr{P}_{\mathcal{H}}} |v|^2_{m,K} \right)^{\frac{1}{2}} \quad \text{and} \quad \|v\|_{m,\mathscr{P}_{\mathcal{H}}} := \left(\sum_{K\in\mathscr{P}_{\mathcal{H}}} \|v\|^2_{m,K} \right)^{\frac{1}{2}},$$

and set $V := H^1(\mathscr{P}_{\mathcal{H}})$ equipped with the norm

$$\|v\|_V := \left(\|\nabla v\|^2_{0,\mathscr{P}_{\mathcal{H}}} + \frac{1}{d^2_{\tilde{\Omega}}} \|v\|^2_{0,\mathscr{P}_{\mathcal{H}}} \right)^{\frac{1}{2}}, \tag{1.5}$$

for all $v \in V$. Here, $d_{\tilde{\Omega}} > 0$ is a constant that depends on the domain Ω, and that will be specified later. In addition, we define the inner product

$$(u,v)_{\mathscr{P}_{\mathcal{H}}} := \sum_{K\in\mathscr{P}_{\mathcal{H}}} (u,v)_K, \quad \text{for all } u,v \in V.$$

Since the aim of this work is to introduce a new hybrid formulation, we shall need an appropriate space for the Lagrange multipliers. The natural space in our case consists of functions that are normal traces of $H(\mathrm{div};\Omega)$ functions; more precisely, we define the space

$$\Lambda := \left\{ \boldsymbol{q}\cdot\boldsymbol{n}^K|_{\partial K}, \text{ for all } K \in \mathscr{P}_{\mathcal{H}} \ : \ \boldsymbol{q} \in H(\mathrm{div};\Omega) \right\}, \tag{1.6}$$

equipped with the norm

$$\|\mu\|_\Lambda := \inf \{ \|\boldsymbol{q}\|_{\mathrm{div},\Omega} : \boldsymbol{q} \in H(\mathrm{div};\Omega) \text{ and } \boldsymbol{q}\cdot\boldsymbol{n}^K|_{\partial K} = \mu, \forall K \in \mathscr{P}_{\mathcal{H}} \}, \tag{1.7}$$

with,

$$\|\boldsymbol{p}\|_{\mathrm{div},\Omega} := \left(\|\boldsymbol{p}\|^2_{0,\Omega} + d^2_{\tilde{\Omega}} \|\nabla\cdot\boldsymbol{p}\|^2_{0,\Omega} \right)^{\frac{1}{2}}, \text{ for all } \boldsymbol{p} \in H(\mathrm{div};\Omega).$$

Denoting by $\langle\cdot,\cdot\rangle_{\partial K}$ the duality pairing between $H^{-\frac{1}{2}}(\partial K)$ and $H^{\frac{1}{2}}(\partial K)$, the Trace Theorem (see, e.g., [17, Theorem 3.10]) ensures that the following *duality pairing* between $\prod_{K\in\mathscr{P}_{\mathcal{H}}} H^{-\frac{1}{2}}(\partial K)$ and V is well-defined:

$$\langle\mu,v\rangle_{\partial\mathscr{P}_{\mathcal{H}}} := \sum_{K\in\mathscr{P}_{\mathcal{H}}} \langle\mu,v\rangle_{\partial K}, \quad \text{for all } (\mu,v) \in \prod_{K\in\mathscr{P}_{\mathcal{H}}} H^{-\frac{1}{2}}(\partial K) \times V. \tag{1.8}$$

Moreover, the following identity can be proven as in [20, pp. 5]

$$\|\mu\|_\Lambda = \sup_{v\in V} \frac{\langle\mu,v\rangle_{\partial\mathscr{P}_{\mathcal{H}}}}{\|v\|_V}, \text{ for all } \mu \in \Lambda. \tag{1.9}$$

Here, and thereafter, we lighten the notation by writing $\sup_{v\in V}$ instead of $\sup_{v\in V\setminus\{\mathbf{0}\}}$.

Finally, associated to $\mathcal{E}_H$ and $\mathscr{T}_h^K$, for $\ell \geq 0$, we introduce the following finite element spaces:

$$\Lambda_H := \{\mu_H \in \Lambda : \mu_H|_F \in \mathbb{P}_\ell(F), \forall F \in \mathcal{E}_H\}, \tag{1.10}$$

$$V_h(K) := \{v_h \in \mathcal{C}^0(K) : v_h|_{\mathfrak{T}} \in \mathbb{P}_k(\mathfrak{T}), \forall \mathfrak{T} \in \mathscr{T}_h^K\}, \tag{1.11}$$

$$V_h := \prod_{K\in\mathscr{P}_{\mathcal{H}}} V_h(K). \tag{1.12}$$

We close this section by presenting in Table 1 a summary of the different partitions and spaces used to construct the method.

Partition	Definition	Associated Space	
$\mathscr{P}_{\mathcal{H}}$	Partition for Ω	$u \in V := H^1(\mathscr{P}_{\mathcal{H}})$	(•)
$\mathcal{E}$	Collection of facets of $\mathscr{P}_{\mathcal{H}}$	$\lambda \in \Lambda$ - see (1.6)	(•)
$\mathcal{E}_H$	Partitions on each facet in $\mathcal{E}$	$\lambda_H \in \Lambda_H$ - see (1.10)	(♠)
$\mathscr{T}_h$	Triangulations on each polytope in $\mathscr{P}_{\mathcal{H}}$	$u_h \in V_h$ - see (1.12)	(♣)

TABLE 1

Summary of partitions and spaces. (•) The coarse partition $\mathscr{P}_{\mathcal{H}}$ and its facets $\mathcal{E}$. (♠) First level of discretization. (♣) Second level of discretization.

2. A new Hybrid Formulation. As it was mentioned in the introduction, the starting point in building the method is to derive an equivalent weak formulation of (1.1) based on a hybridization procedure. Our presentation below borrows ideas from [25, 3, 8], which in turn are inspired by [37]. First, the standard weak formulation of (1.1) is given by: *Find $u \in H^1_0(\Omega)$ such that*

$$(\mathcal{K}\nabla u\,,\nabla v)_\Omega = (f,v)_\Omega\,,\ \text{for all } v \in H^1_0(\Omega)\,. \tag{2.1}$$

We shall propose a hybrid weak formulation, equivalent to (2.1). The first ingredient is a linear mapping $\varsigma : V \to H^{-\frac{1}{2}}(\partial\mathscr{P}_{\mathcal{H}})$ that, for now, will only be required to be continuous, and satisfy

$$v \in H^1_0(\Omega) \Rightarrow \varsigma(v) \in \Lambda\,. \tag{2.2}$$

Using this mapping, we propose the following hybrid variational formulation: *Find $(u,\,\lambda) \in V \times \Lambda$ such that*

$$\begin{cases} a(u,v) + \langle\lambda, v\rangle_{\partial\mathscr{P}_{\mathcal{H}}} = (f,v)_{\mathscr{P}_{\mathcal{H}}}\,,\ \text{for all } v \in V \\ \qquad\quad \langle\mu, u\rangle_{\partial\mathscr{P}_{\mathcal{H}}} = 0\,,\ \text{for all } \mu \in \Lambda \end{cases}\,, \tag{2.3}$$

where the bilinear form $a(\cdot,\cdot) : V \times V \to \mathbb{R}$ is defined by,

$$a(w,v) := (\mathcal{K}\nabla w, \nabla v)_{\mathscr{P}_{\mathcal{H}}} + \langle\varsigma(w)\,, v\rangle_{\partial\mathscr{P}_{\mathcal{H}}}\,. \tag{2.4}$$

Notice that if ς is identically zero, then (2.3) is the classical hybrid formulation proposed in [37] and the rest of the derivation would coincide with what was presented in [3]. So, following ideas from [3, 8] we now prove that (2.1) and (2.3) are equivalent.

THEOREM 2.1. *The function $u \in H^1_0(\Omega)$ solves (2.1) if and only if $(u,\lambda) \in V \times \Lambda$ solves (2.3). Moreover, the following relation between u and λ holds*

$$\lambda = (-\mathcal{K}\nabla u \cdot \boldsymbol{n}^K - \varsigma(u))|_{\partial K}\,,\ \textit{for all } K \in \mathscr{P}_{\mathcal{H}}. \tag{2.5}$$

Proof. Let $(u,\lambda) \in V \times \Lambda$ be a solution of (2.3). Using [36, Lemma 1] the following characterization holds

$$H^1_0(\Omega) = \{v \in V : \langle\mu\,, v\rangle_{\partial\mathscr{P}_{\mathcal{H}}} = 0\,,\ \text{for all } \mu \in \Lambda\}\,. \tag{2.6}$$

So, using the second equation in (2.3) we conclude that $u \in H^1_0(\Omega)$ and $\varsigma(u) \in \Lambda$. Hence $\langle\varsigma(u)\,, v\rangle_{\partial\mathscr{P}_{\mathcal{H}}} = 0$, for all $v \in H^1_0(\Omega)$, and the first equation in (2.3) implies that

$$(\mathcal{K}\nabla u\,,\nabla v)_\Omega \;=\; (f\,,v)_\Omega\,,\ \text{for all } v \in H^1_0(\Omega)\,,$$

and thus u solves (2.1).

Conversely, let $u \in H_0^1(\Omega)$ be the solution of (2.1) and let us consider the following continuous linear functional on V

$$L(v) = (f, v)_{\partial\mathscr{P}_\mathcal{H}} - (\mathcal{K}\nabla u\,, \nabla v)_{\partial\mathscr{P}_\mathcal{H}} - \langle \varsigma(u)\,, v\rangle_{\partial\mathscr{P}_\mathcal{H}}\,. \tag{2.7}$$

This functional vanishes on $H_0^1(\Omega)$; so, thanks to the inf-sup condition (1.9) there exists a unique $\lambda \in \Lambda$ such that

$$\langle \lambda, v\rangle_{\partial\mathscr{P}_\mathcal{H}} = L(v)\,, \text{ for all } v \in V.$$

Hence, the pair $(u, \lambda) \in V \times \Lambda$ solves (2.3).

Finally, since $f = \operatorname{div}(-\mathcal{K}\nabla u)$, replacing and integrating by parts in (2.7), we arrive at

$$L(v) = \sum_{K\in\mathscr{P}_\mathcal{H}} -\langle \mathcal{K}\nabla u\cdot \boldsymbol{n}^K + \varsigma(u)\,, v\rangle_{\partial K} = \langle \lambda\,, v\rangle_{\partial\mathscr{P}_\mathcal{H}}\,,$$

which proves (2.5). ∎

2.1. Explicit definition of $\varsigma(\cdot)$. The result given by Theorem 2.1 provides existence and uniqueness of solution for (2.3), as long as $\varsigma(\cdot)$ satisfies (2.2). So, this condition needs to be kept in mind when defining a concrete mapping $\varsigma(\cdot)$. Let us consider $\boldsymbol{\sigma} \in W^{1,\infty}(\Omega)^d$ and $v \in V$. It is easy to notice that $v\,\boldsymbol{\sigma}|_K \in H(\operatorname{div}; K)$ for all $K \in \mathscr{P}_\mathcal{H}$. Moreover, if $v \in H_0^1(\Omega)$ then $v\,\boldsymbol{\sigma} \in H(\operatorname{div}; \Omega)$. Thus, the following is a valid definition for ς:

$$\begin{aligned} &\varsigma : V \to H^{-\frac{1}{2}}(\partial\mathscr{P}_\mathcal{H})\,,\\ &\quad v \mapsto \varsigma(v)|_{\partial K} := (v\,\boldsymbol{\sigma})|_{\partial K}\cdot \boldsymbol{n}^K\,, \text{ in each } K \in \mathscr{P}_\mathcal{H}\,. \end{aligned} \tag{2.8}$$

Now, we give a concrete definition of $\boldsymbol{\sigma} \in W^{1,\infty}(\Omega)^d$ that will ensure that the bilinear form $a(\cdot,\cdot)$ is elliptic. Let us define an open and bounded rectangular parallelepiped

$$\tilde{\Omega} = \Pi_{i=1}^d (a_i\,, b_i) \subset \mathbb{R}^d\,,$$

such that $\bar{\Omega} \subset \tilde{\Omega}$. In what follows we denote $\boldsymbol{\sigma}(\boldsymbol{x}) = (\sigma_1(\boldsymbol{x}), \ldots, \sigma_d(\boldsymbol{x}))$ where $\boldsymbol{x} = (x_1, \ldots, x_d) \in \tilde{\Omega}$. Then, for $j \in \{1, \ldots, d\}$ we define:

$$\sigma_j(\boldsymbol{x}) := \frac{\nu}{d}\,(x_j - a_j)\,, \text{ for all } \boldsymbol{x} \in \tilde{\Omega}\,, \tag{2.9}$$

where $\nu > 0$ will be chosen later. The function $\boldsymbol{\sigma}$ just defined satisfies the following important properties

$$\operatorname{div}\boldsymbol{\sigma}\,(\boldsymbol{x}) = \sum_{j=1}^d \partial_{x_j}\sigma_j\,(\boldsymbol{x}) = \sum_{j=1}^d \frac{\nu}{d} = \nu\,, \tag{2.10}$$

and

$$\|\boldsymbol{\sigma}\|_{0,\infty,\Omega} = \operatorname*{ess\,sup}_{\boldsymbol{x}\in\Omega} \left(\sum_{j=1}^d |\sigma_j(\boldsymbol{x})|^2\right)^{\frac{1}{2}} \le \nu \max_{j\in\{1,\ldots,d\}} |b_j - a_j| \le d_{\tilde{\Omega}}\,\nu\,, \tag{2.11}$$

where $d_{\tilde{\Omega}} > 0$ is the diameter of $\tilde{\Omega}$. Then, using the above definitions the bilinear form $a(\cdot,\cdot)$ can be expressed in the following equivalent ways:

$$a(u,v) = (\mathcal{K}\nabla u, \nabla v)_{\mathscr{P}_\mathcal{H}} + \langle (u\boldsymbol{\sigma})\cdot \boldsymbol{n}^K, v\rangle_{\partial\mathscr{P}_\mathcal{H}} \tag{2.12}$$

$$= (\mathcal{K}\nabla u, \nabla v)_{\mathscr{P}_\mathcal{H}} + (\boldsymbol{\sigma}\cdot\nabla u\,, v)_{\mathscr{P}_\mathcal{H}} + (u\,, \boldsymbol{\sigma}\cdot\nabla v)_{\mathscr{P}_\mathcal{H}} + \nu\,(u\,,v)_{\mathscr{P}_\mathcal{H}}\,. \tag{2.13}$$

The aforementioned ellipticity of $a(\cdot,\cdot)$ as well as its continuity are established in the following result.

THEOREM 2.2. *Let us suppose that, in the definition of (2.9), ν is chosen such that*

$$0 \le \nu \le \frac{\mathcal{K}_{\min}}{4\,d_{\tilde{\Omega}}^2}\,. \tag{2.14}$$

Then, the bilinear form $a(\cdot,\cdot)$ defined in (2.12) is continuous and elliptic. More precisely, for all $v, w \in V$ the following holds

$$a(w\,,v) \le 2\,\left(\|\mathcal{K}^{\frac{1}{2}}\,\nabla w\|^2_{0,\mathscr{P}_\mathcal{H}} + \nu\,\|w\|^2_{0,\mathscr{P}_\mathcal{H}}\right)^{\frac{1}{2}}\,\left(\|\mathcal{K}^{\frac{1}{2}}\,\nabla v\|^2_{0,\mathscr{P}_\mathcal{H}} + \nu\,\|v\|^2_{0,\mathscr{P}_\mathcal{H}}\right)^{\frac{1}{2}}\,,$$

$$a(v\,,v) \ge \frac{1}{2}\,\left(\|\mathcal{K}^{\frac{1}{2}}\,\nabla v\|^2_{0,\mathscr{P}_\mathcal{H}} + \nu\,\|v\|^2_{0,\mathscr{P}_\mathcal{H}}\right)\,.$$

Proof. Let $w, v \in V$. Using the writing (2.13) for $a(\cdot,\cdot)$, Cauchy-Schwarz's inequality, (2.10), and (2.11) we arrive at

$$\begin{aligned}
a(w,v) &= (\mathcal{K}^{\frac{1}{2}}\,\nabla w\,, \mathcal{K}^{\frac{1}{2}}\,\nabla v)_{\mathscr{P}_\mathcal{H}} + (\boldsymbol{\sigma}\cdot\nabla w\,, v)_{\mathscr{P}_\mathcal{H}} + (w\,, \boldsymbol{\sigma}\cdot\nabla v)_{\mathscr{P}_\mathcal{H}} + \nu\,(w\,,v)_{\mathscr{P}_\mathcal{H}} \\
&\le \|\mathcal{K}^{\frac{1}{2}}\,\nabla w\|_{0,\mathscr{P}_\mathcal{H}}\,\|\mathcal{K}^{\frac{1}{2}}\,\nabla v\|_{0,\mathscr{P}_\mathcal{H}} + \nu\,\|w\|_{0,\mathscr{P}_\mathcal{H}}\,\|v\|_{0,\mathscr{P}_\mathcal{H}} \\
&\quad + \frac{1}{2}\,\nu^{\frac{1}{2}}\,(\|\mathcal{K}^{\frac{1}{2}}\,\nabla w\|_{0,\mathscr{P}_\mathcal{H}}\,\|v\|_{0,\mathscr{P}_\mathcal{H}} + \|w\|_{0,\mathscr{P}_\mathcal{H}}\,\|\mathcal{K}^{\frac{1}{2}}\,\nabla v\|_{0,\mathscr{P}_\mathcal{H}}) \\
&\le \left(\|\mathcal{K}^{\frac{1}{2}}\,\nabla w\|_{0,\mathscr{P}_\mathcal{H}} + \nu^{\frac{1}{2}}\,\|w\|_{0,\mathscr{P}_\mathcal{H}}\right)\,\left(\|\mathcal{K}^{\frac{1}{2}}\,\nabla v\|_{0,\mathscr{P}_\mathcal{H}} + \nu^{\frac{1}{2}}\,\|v\|_{0,\mathscr{P}_\mathcal{H}}\right) \\
&\le 2\,\left(\|\mathcal{K}^{\frac{1}{2}}\,\nabla w\|^2_{0,\mathscr{P}_\mathcal{H}} + \nu\,\|w\|^2_{0,\mathscr{P}_\mathcal{H}}\right)^{\frac{1}{2}}\,\left(\|\mathcal{K}^{\frac{1}{2}}\,\nabla v\|^2_{0,\mathscr{P}_\mathcal{H}} + \nu\,\|v\|^2_{0,\mathscr{P}_\mathcal{H}}\right)^{\frac{1}{2}}\,,
\end{aligned}$$

and,

$$\begin{aligned}
a(v,v) =&\ (\mathcal{K}\,\nabla v\,, \nabla v)_{\mathscr{P}_\mathcal{H}} + 2\,(\boldsymbol{\sigma}\cdot\nabla v\,, v)_{\mathscr{P}_\mathcal{H}} + \nu\,(v,v)_{\mathscr{P}_\mathcal{H}} \\
\ge&\ \|\mathcal{K}^{\frac{1}{2}}\nabla v\|^2_{0,\mathscr{P}_\mathcal{H}} - 2\,d_{\tilde{\Omega}}\,\nu\,|v|_{1,\mathscr{P}_\mathcal{H}}\,\|v\|_{0,\mathscr{P}_\mathcal{H}} + \nu\,\|v\|^2_{0,\mathscr{P}_\mathcal{H}} \\
\ge&\ \frac{1}{2}\,\left(\|\mathcal{K}^{\frac{1}{2}}\,\nabla v\|^2_{0,\mathscr{P}_\mathcal{H}} + \nu\,\|v\|^2_{0,\mathscr{P}_\mathcal{H}}\right) + \nu\,\left(\sqrt{2}\,d_{\tilde{\Omega}}\,|v|_{1,\mathscr{P}_\mathcal{H}} - \frac{1}{\sqrt{2}}\,\|v\|_{0,\mathscr{P}_\mathcal{H}}\right)^2 \\
\ge&\ \frac{1}{2}\,\left(\|\mathcal{K}^{\frac{1}{2}}\,\nabla v\|^2_{0,\mathscr{P}_\mathcal{H}} + \nu\,\|v\|^2_{0,\mathscr{P}_\mathcal{H}}\right)\,,
\end{aligned}$$

which proves the Theorem. ∎

To link the ellipticity and continuity of $a(\cdot,\cdot)$ just proved with the norm $\|\cdot\|_V$, we note that using (2.14) we obtain

$$a(w,v) \le 2\,\mathcal{K}_{\max}\,\|w\|_V\,\|v\|_V\,, \text{and, } a(v,v) \ge \frac{1}{2}\nu\,d_{\tilde{\Omega}}^2\,\|v\|_V^2\,, \text{ for all } w, v \in V\,. \tag{2.15}$$

Interestingly, the bilinear form $a(\cdot,\cdot)$ is elliptic in $H^1_0(\Omega)$ even if $\nu = 0$. It is therefore sufficient to use the standard theory for variational problems with constraints, which is precisely what the next theorem shows.

THEOREM 2.3. *Suppose that, in the definition of (2.9), ν is chosen such that (2.14) holds. Then, problem (2.3) has a unique solution $(u\,,\lambda) \in V \times \Lambda$. Moreover, the following stability holds*

$$\|\lambda\|_{\Lambda} + \mathcal{K}_{max}\,\|u\|_V \leq C\,\frac{\mathcal{K}_{max}}{\mathcal{K}_{min}}\,\|f\|_{0,\Omega}\,, \tag{2.16}$$

where, $C > 0$ does not depend on any mesh size, data of the problem, or ν.

Proof. The existence and uniqueness of the solution to (2.3) is a consequence of its equivalence with (2.1) and the fact that the latter has a unique solution. The remaining part of the proof is related to giving the bound (2.16). We first notice that for all $v \in H^1_0(\Omega)$ we have $\|v\|_{0,\Omega} \leq c_P\,\|\nabla v\|_{0,\Omega}$, where the Poincaré constant $c_P > 0$ depends only on Ω. Thus, from the ellipticity given in Theorem 2.2 and the fact that $c_P \leq d_{\tilde{\Omega}}$ we arrive at

$$a(v,v) \geq \frac{1}{2}\,\mathcal{K}_{\min}\,\|v\|^2_V\,, \quad \text{for all } v \in H^1_0(\Omega).$$

Then,

$$\frac{1}{2}\,\mathcal{K}_{\min}\,\|u\|^2_V \leq a(u,u) = (f,u)_{0,\mathscr{P}_{\mathcal{H}}} \leq c_P\,\|f\|_{0,\Omega}\,\|u\|_V\,.$$

So, using (2.15) and the inf-sup condition (1.9) we get

$$\|\lambda\|_{\Lambda} = \sup_{v\in V}\frac{\langle \lambda\,, v\rangle_{\partial\mathscr{P}_{\mathcal{H}}}}{\|v\|_V} = \sup_{v\in V}\frac{(f,v)_{0,\mathscr{P}_{\mathcal{H}}} - a(u,v)}{\|v\|_V} \leq c_P\,\|f\|_{0,\Omega} + 2\,\mathcal{K}_{\max}\,\|u\|_V\,.$$

The proof is finished by combining the above bounds. ∎

Remark 2.4. Although the equivalence result presented in Theorem 2.1 holds for any choice of mapping $\varsigma(\cdot)$, the uniform stability (with respect to ν) on the solution of the hybrid problem (2.3) is due to the precise choice of $\boldsymbol{\sigma}$ done in this work. More general definitions of $\varsigma(\cdot)$ could be considered leading to related stability results, based this time in inf-sup conditions for $a(\cdot,\cdot)$, but in such a case the uniform stability with respect to $\varsigma(\cdot)$ would no longer be guaranteed.

2.2. The discrete hybrid problem. We start by recalling the definition of the spaces V_h and Λ_H given in (1.12) and (1.10). The Galerkin discretization of (2.3) using these spaces reads as follows: *Find $(u_h\,,\lambda_H) \in V_h \times \Lambda_H$ such that*

$$\begin{cases} a(u_h,v_h) + \langle \lambda_H, v_h\rangle_{\partial\mathscr{P}_{\mathcal{H}}} \;=\; (f,v_h)_{\mathscr{P}_{\mathcal{H}}}\,, \text{ for all } v_h \in V_h \\ \qquad\qquad \langle \mu_H, u_h\rangle_{\partial\mathscr{P}_{\mathcal{H}}} \;=\; 0\,, \text{ for all } \mu_H \in \Lambda_H \end{cases}. \tag{2.17}$$

The first step in analyzing the discrete problem is to define the discrete kernel

$$\mathfrak{N}_h := \{v_h \in V_h : \langle \mu_H, v_h\rangle_{\partial\mathscr{P}_{\mathcal{H}}} = 0\,, \forall\, \mu_H \in \Lambda_H\}\,. \tag{2.18}$$

Then, the Poincaré–Friedrichs inequality for piecewise H^1 functions given in [9, Eq. (1.3)] implies the existence of $c_B > 0$ that depends only on the shape of the polygons of $\mathscr{P}_{\mathcal{H}}$ (and not on h, H, or $\mathcal{H}$) such that

$$\|v_h\|_{0,\Omega} \leq c_B\,\|\nabla v_h\|_{0,\mathscr{P}_{\mathcal{H}}}\,, \text{ for all } v_h \in \mathfrak{N}_h\,. \tag{2.19}$$

So, $v_h \mapsto \|\mathcal{K}^{\frac{1}{2}}\nabla v_h\|_{0,\mathscr{P}_\mathcal{H}}$ is a norm on $\mathfrak{N}_h$. This observation also allows us to make the ellipticity in Theorem 2.2 more precise. In fact, the ellipticity in Theorem 2.2 implies:

$$a(v_h, v_h) \geq \frac{1}{2}\left(\|\mathcal{K}^{\frac{1}{2}}\nabla v_h\|^2_{0,\mathscr{P}_\mathcal{H}} + \nu\,\|v_h\|^2_{0,\mathscr{P}_\mathcal{H}}\right) \geq \frac{1}{2}\,\|\mathcal{K}^{\frac{1}{2}}\nabla v_h\|^2_{0,\mathscr{P}_\mathcal{H}}\,, \tag{2.20}$$

for all $v_h \in \mathfrak{N}_h$, which is indeed an ellipticity in the discrete kernel $\mathfrak{N}_h$. Moreover, thanks to the Poincaré inequality (2.19) we have

$$a(v_h, v_h) \geq \frac{1}{2}\left(\frac{d^2_{\tilde{\Omega}}}{d^2_{\tilde{\Omega}} + c_B^2}\right)\mathcal{K}_{\min}\,\|v_h\|^2_V\,. \tag{2.21}$$

In addition, the hypotheses made in subsection 1.3 on the partitions $\mathscr{P}_\mathcal{H}$ and $\mathscr{T}_h$ allow us to use the results from [8] and [20] to prove the following discrete inf-sup condition:

$$\frac{1}{c_F}\,\|\mu_H\|_\Lambda \leq \sup_{v_h\in V_h}\frac{\langle \mu_H, v_h\rangle_{\partial\mathscr{P}_\mathcal{H}}}{\|v_h\|_V}\,, \tag{2.22}$$

where $c_F > 0$ is independent of h, H, and $\mathcal{H}$. As a consequence, the finite element method (2.17) is well-posed, and has stability and error constants independent of ν. This is stated in the following result.

THEOREM 2.5. *There exists a unique $(u_h\,, \lambda_H) \in V_h \times \Lambda_H$ that is the solution to (2.17). In addition, the discrete solution satisfies the following stability*

$$\frac{1}{c_F}\,\|\lambda_H\|_\Lambda + \mathcal{K}_{max}\,\|u_h\|_V \leq C\,\frac{\mathcal{K}_{max}}{\mathcal{K}_{min}}\,\|f\|_{0,\Omega}\,, \tag{2.23}$$

where, $C > 0$ does not depend on any mesh size, data, or ν. Moreover we have the following error estimate

$$\|u - u_h\|_V \leq c_1 \inf_{v_h\in V_h}\|u - v_h\|_V + c_2 \inf_{\rho_H\in\Lambda_H}\|\lambda - \rho_H\|_\Lambda\,, \tag{2.24}$$

$$\|\lambda - \lambda_H\|_\Lambda \leq c_3 \inf_{v_h\in V_h}\|u - v_h\|_V + c_4 \inf_{\rho_H\in\Lambda_H}\|\lambda - \rho_H\|_\Lambda\,, \tag{2.25}$$

where c_1, c_2, c_3, and c_4 are positive constants independent of mesh sizes, and ν.

Proof. The proof of the existence and uniqueness of solution to (2.17) follows from the ellipticity (2.20) of $a(\cdot,\cdot)$ on $\mathfrak{N}_h$, the discrete inf-sup condition (2.22), and standard results on saddle-point problems (see, e.g., [39, 18]). The stability (2.23) can be obtained following closely the proof of Theorem 2.3. Finally, the error bounds (2.24) and (2.25) are obtained by applying [18, Lemma 50.2]. ∎

The Cea-like estimates (2.24) and (2.25) lead to optimal-order error estimates. For this, we first state the following result, whose proof is a slight variation of that from [8, Lemma 3].

LEMMA 2.6. *Suppose $w \in H^{\ell+2}(\mathscr{P}_\mathcal{H}) \cap H^1_0(\Omega)$, $\mathcal{K}\nabla w \in H^{\ell+1}(\mathscr{P}_\mathcal{H})$, with $\ell \geq 0$, and $\mathcal{K}\nabla w \in H(\mathrm{div};\Omega)$. Let $\mu \in \Lambda$ defined by*

$$\mu|_E = -\left(\mathcal{K}\nabla w\cdot \boldsymbol{n}^K + w\,(\boldsymbol{\sigma}\cdot\boldsymbol{n}^K)\right)|_E$$

for each $E \in \mathcal{E}$. Then, there exists a positive constant $C > 0$, independent of h, H, $\mathcal{H}$, and $\mathcal{K}$, such that

$$\inf_{\mu_H \in \Lambda_H} \|\mu - \mu_H\|_\Lambda \leq C\, H^{\ell+1}\, |\mathcal{K}\nabla w + w\,\boldsymbol{\sigma}|_{\ell+1,\mathscr{P}_\mathcal{H}}\,, \tag{2.26}$$

where Λ_H and $\boldsymbol{\sigma} \in [\mathcal{C}^\infty(\Omega)]^d$ are given in (1.10) and (2.9), respectively.

The last approximation result, along with standard interpolation estimates (see, e.g., [17]) lead, in a natural way, to the following error estimate for the discrete hybrid problem (2.17).

COROLLARY 2.7. *Suppose that the solution (u, λ) of (2.3) satisfies the hypotheses of Lemma 2.6. Then, there exist positive constants C_1, C_2, independent of any mesh size and ν, such that*

$$\|u - u_h\|_V \leq C_1 \left(H^{\ell+1}\, |\mathcal{K}\nabla u + u\,\boldsymbol{\sigma}|_{\ell+1,\mathscr{P}_\mathcal{H}} + h^k\, |u|_{k+1,\mathscr{P}_\mathcal{H}} \right)\,, \tag{2.27}$$

$$\|\lambda - \lambda_H\|_\Lambda \leq C_2 \left(H^{\ell+1}\, |\mathcal{K}\nabla u + u\,\boldsymbol{\sigma}|_{\ell+1,\mathscr{P}_\mathcal{H}} + h^k\, |u|_{k+1,\mathscr{P}_\mathcal{H}} \right)\,. \tag{2.28}$$

Remark 2.8. We stress the robustness of the error constants with respect to ν. As a matter of fact, the only dependence on ν that appears on the error is via the term $|u\boldsymbol{\sigma}|_{\ell+1,\Omega}$ on the right-hand side of (2.27),(2.28). This dependence is nevertheless very weak, for two related reasons. First, the definition (2.9) of $\boldsymbol{\sigma}$ implies that $|\boldsymbol{\sigma}|_{s,\Omega} = 0$ for any $s \geq 2$. So, that term is (up to a constant that depends only on Ω) bounded by $\nu\, \|u\|_{\ell+1,\mathscr{P}_\mathcal{H}}$. In addition, the restriction the value of ν given in Theorem 2.2 implies the following uniform bound:

$$|u\boldsymbol{\sigma}|_{\ell+1,\mathscr{P}_\mathcal{H}} \leq C\, \frac{\mathcal{K}_{\min}}{4\, d_{\tilde{\Omega}}^2}\, \|u\|_{\ell+1,\mathscr{P}_\mathcal{H}}\,, \tag{2.29}$$

where $C > 0$ depends only on the diameter of Ω, and in ℓ.

Remark 2.9. Regarding the regularity requirements for the error analysis, it is important to notice two things. First, the best approximation result from Theorem 2.5 is totally independent of the regularity of the diffusion tensor $\mathcal{K}$, so it does imply convergence for the lowest regularity case. In addition, the bounds (2.27),(2.28) do require a regularity on $\mathcal{K}$, but only locally. In fact, the freedom to choose the shape of the elements in $\mathscr{P}_\mathcal{H}$ allows for obtaining optimal error estimates as long as $\mathcal{K}$ is smooth in each element $K \in \mathscr{P}_\mathcal{H}$.

The fact that the stability and error results just proven are robust with respect to ν prompts the question of what happens in the limit $\nu \to 0$. It is important to notice that for $\nu = 0$ the discrete problem (2.17) is, in fact, equivalent to the MHM method proposed in [8], and so the limit problem when $\nu = 0$ has a unique solution as well. To explain the transition between the two cases ($\nu \neq 0$ and $\nu = 0$), in the next result we study the convergence of u_h as $\nu \to 0$, and provide an uper bound for the error.

THEOREM 2.10. *Let $(u_h\,, \lambda_H) \in V_h \times \Lambda_H$ be the solution of (2.17), and let us denote the solution of (2.17) when $\nu = 0$ by $(u_h^0\,, \lambda_H^0)$. Then, there exists a constant C, independent of ν, and every physical and mesh parameters, such that*

$$\|\mathcal{K}^{\frac{1}{2}}\, \nabla(u_h - u_h^0)\|_{0,\mathscr{P}_\mathcal{H}} \leq C\, \frac{1}{\mathcal{K}_{min}^{\frac{3}{2}}}\, \nu\, \|f\|_{0,\Omega}\,. \tag{2.30}$$

Proof. Let $e_h := u_h - u_h^0$. Since both u_h and u_h^0 belong to $\mathfrak{N}_h$, using (2.17) we get

$$a(u_h, e_h) = (f, e_h)_{\mathscr{P}_\mathcal{H}} = (\mathcal{K}\nabla u_h^0, \nabla e_h)_{\mathscr{P}_\mathcal{H}} = a(u_h^0, e_h) - \langle (u_h^0 \boldsymbol{\sigma}) \cdot \boldsymbol{n}^K, e_h \rangle_{\partial \mathscr{P}_\mathcal{H}} .$$

Rearranging terms, using (2.13), (2.10), (2.11), (2.23), and (2.19), we arrive at

$$\begin{aligned} \frac{1}{2} \|\mathcal{K}^{\frac{1}{2}} \nabla e_h\|^2_{0,\mathscr{P}_\mathcal{H}} &\leq a(e_h, e_h) \\ &= - \langle (u_h^0 \boldsymbol{\sigma}) \cdot \boldsymbol{n}^K, e_h \rangle_{\partial \mathscr{P}_\mathcal{H}} \\ &= - \left[(\boldsymbol{\sigma} \cdot \nabla u_h^0, e_h)_{\mathscr{P}_\mathcal{H}} + (u_h^0, \boldsymbol{\sigma} \cdot \nabla e_h)_{\mathscr{P}_\mathcal{H}} + ((\nabla \cdot \boldsymbol{\sigma})\, u_h^0, e_h)_{\mathscr{P}_\mathcal{H}} \right] \\ &\leq \sqrt{2}\, (d_{\tilde{\Omega}}^2 + d_{\tilde{\Omega}}\, c_B) \, \frac{1}{\mathcal{K}_{\min}^{\frac{1}{2}}} \, \nu \, \|u_h^0\|_V \, \|\mathcal{K}^{\frac{1}{2}} \nabla e_h\|_{0,\mathscr{P}_\mathcal{H}} , \end{aligned}$$

yielding

$$\|\mathcal{K}^{\frac{1}{2}} \nabla e_h\|_{0,\mathscr{P}_\mathcal{H}} \leq 2\sqrt{2}\, (d_{\tilde{\Omega}}^2 + d_{\tilde{\Omega}}\, c_B) \, \frac{1}{\mathcal{K}_{\min}^{\frac{1}{2}}} \, \nu \, \|u_h^0\|_V . \tag{2.31}$$

Finally, from the definition of u_h^0 and (2.21) we arrive at:

$$\|u_h^0\|_V \leq 2 \left(1 + \frac{c_B^2}{d_{\tilde{\Omega}}^2} \right) d_{\tilde{\Omega}} \, \frac{1}{\mathcal{K}_{\min}} \, \|f\|_{0,\Omega} . \tag{2.32}$$

Therefore, inserting (2.32) in (2.31) we get

$$\|\mathcal{K}^{\frac{1}{2}} \nabla e_h\|_{0,\mathscr{P}_\mathcal{H}} \leq C \, \frac{1}{\mathcal{K}_{\min}^{\frac{3}{2}}} \, \nu \, \|f\|_{0,\Omega} ,$$

which finishes the proof. ∎

3. The Multiscale Hybrid Method. A common feature in all the works related to the MHM method is a process of static condensation. The purpose of this feature is twofold; first, it allows for a natural upscaling to be carried out in parallel, and second, it leads in a natural way to a formulation whose only unknowns are the approximation of the fluxes in the interelement facets, that is, a global linear system with λ_H as the sole unknown. So, we now describe that process in the context of the present approach. We start by observing that the first equation of (2.17) can be rewritten as follows:

$$a(u_h\,, v_h) = -\langle \lambda_H, v_h \rangle_{\partial \mathscr{P}_\mathcal{H}} + (f, v_h)_{\mathscr{P}_\mathcal{H}} . \tag{3.1}$$

Due to the linearity of the above problem and the fact that $a(\cdot, \cdot)$ is an elliptic bilinear form, the solution $u_h \in V_h$ of (2.17) can be written in the following way

$$u_h = T_h \lambda_H + \hat{T}_h f\,, \tag{3.2}$$

where $\hat{T}_h f \in V_h$ and $T_h \rho \in V_h$ (for any $\rho \in \Lambda$) are the unique solutions to the following discrete problems:

$$a(T_h\, \rho\,, v_h) = - \langle \rho\,, v_h \rangle_{\partial \mathscr{P}_\mathcal{H}} , \text{ for all } v_h \in V_h\,, \tag{3.3}$$

$$a(\hat{T}_h\, f\,, v_h) = (f, v_h)_{\mathscr{P}_\mathcal{H}} , \text{ for all } v_h \in V_h\,. \tag{3.4}$$

The ellipticity of $a(\cdot,\cdot)$ in V_h yields the fact that the mappings T_h and $\hat{T}_h$ are well-defined. The writing (3.2) constitutes a static condensation procedure. In fact, as it will be detailed in Remark 3.3, the mappings T_h and $\hat{T}_h$ can be computed locally. These local computations allow the elimination of the degrees of freedom internal to each element, so that we can write the global problem only in terms of λ_H. The final step in the derivation of the Multiscale Hybrid (MH) method is to replace (3.2) in the second equation of (2.17) to arrive at the following equation involving only λ_H: *Find* $\lambda_H \in \Lambda_H$ *such that*

$$\mathfrak{B}(\lambda_H, \mu_H) = \langle \mu_H \, , \hat{T}_h \, f \rangle_{\partial \mathscr{P}_\mathcal{H}} \, , \text{ for all } \mu_H \in \Lambda_H \, , \tag{3.5}$$

where the bilinear form $\mathfrak{B}$ is given by

$$\mathfrak{B}(\rho_H, \mu_H) = - \langle \mu_H \, , T_h \rho_H \rangle_{\partial \mathscr{P}_\mathcal{H}} \, , \text{ for all } (\rho_H \, , \mu_H) \in \Lambda_H \times \Lambda_H \, . \tag{3.6}$$

The problems (3.5) and (2.17) are equivalent. Thus, Problem (3.5) has a unique solution $\lambda_H \in \Lambda_H$. Once λ_H is computed, then u_h is built using (3.2). As it will be detailed in the next section, this does not involve any extra computation (local or global). In addition, the error estimates proven in subsection 2.2 for the solution of (2.17) are, of course, still valid for u_h built using (3.2).

The MH's global problem (3.5) can be proven well-posed directly. This is stated in the next result.

THEOREM 3.1. *Suppose Assumption (A1) and (2.14) to hold. Then, for all* $\rho_H \, , \mu_H \in \Lambda_H$ *the following holds*

$$\mathfrak{B}(\rho_H, \mu_H) \leq \frac{2}{d_{\bar{\Omega}}^2 \, \nu} \, \|\mu_H\|_\Lambda \, \|\rho_H\|_\Lambda \, , \text{ for all } (\rho_H \, , \mu_H) \in \Lambda_H \times \Lambda_H \, , \tag{3.7}$$

$$\mathfrak{B}(\mu_H, \mu_H) \geq \frac{1}{2 \, c_F^2 \, \mathcal{K}_{max}} \, \|\mu_H\|_\Lambda^2 \, , \text{ for all } \mu_H \in \Lambda_H \, . \tag{3.8}$$

Proof. Let $\mu_H \in \Lambda_H$. Using the inf-sup condition (2.22) (which follows from (A1)) followed by (3.3), the continuity of $a(\cdot,\cdot)$, and (2.14) we get to:

$$\frac{1}{c_F} \, \|\mu_H\|_\Lambda \leq \sup_{v_h \in V_h} \frac{\langle \mu_H, v_h \rangle_{\partial \mathscr{P}_\mathcal{H}}}{\|v_h\|_V} = \sup_{v_h \in V_h} \frac{a(T_h \, \mu_H, v_h)}{\|v_h\|_V} \tag{3.9}$$

$$\leq \mathcal{K}_{\max}^{\frac{1}{2}} \left(\|\mathcal{K}^{\frac{1}{2}} \nabla T_h \, \mu_H\|_{0,\mathscr{P}_\mathcal{H}}^2 + \nu \, \|T_h \, \mu_H\|_{0,\mathscr{P}_\mathcal{H}}^2 \right)^{\frac{1}{2}} \, . \tag{3.10}$$

Then, using the definition of $\mathfrak{B}$, followed by (3.3), and the ellipticity of $a(\cdot,\cdot)$ in Theorem 2.2 we arrive at

$$\begin{aligned} \mathfrak{B}(\mu_H, \mu_H) &= - \langle \mu_H \, , T_h \mu_H \rangle_{\partial \mathscr{P}_\mathcal{H}} = a(T_h \mu_H \, , T_h \mu_H) \\ &\geq \frac{1}{2} \left(\|\mathcal{K}^{\frac{1}{2}} \nabla T_h \, \mu_H\|_{0,\mathscr{P}_\mathcal{H}}^2 + \nu \, \|T_h \, \mu_H\|_{0,\mathscr{P}_\mathcal{H}}^2 \right) \geq \frac{1}{2 \, c_F^2 \, \mathcal{K}_{\max}} \, \|\mu_H\|_\Lambda^2 \, , \end{aligned} \tag{3.11}$$

which proves (3.8). Next, to obtain (3.7) we use again the ellipticity of $a(\cdot,\cdot)$ followed by its continuity to obtain

$$\frac{1}{2} \, d_{\bar{\Omega}}^2 \, \nu \|T_h \, \mu_H\|_V^2 \leq a(T_h \, \mu_H, T_h \, \mu_H) = - \langle \mu_H, T_h \, \mu_H \rangle_{\partial \mathscr{P}_\mathcal{H}} \leq \|\mu_H\|_\Lambda \, \|T_h \, \mu_H\|_V \, ,$$

which proves the following continuity of T_h

$$\|T_h\,\mu_H\|_V \leq \frac{2}{d_{\tilde{\Omega}}^2\,\nu}\,\|\mu_H\|_\Lambda\,.$$

Hence,

$$\mathfrak{B}(\rho_H,\mu_H) = \langle \mu_H\,, T_h\rho_H\rangle_{\partial\mathscr{P}_\mathcal{H}} \leq \|\mu_H\|_\Lambda \|T_h\lambda_H\|_V \leq \frac{2}{d_{\tilde{\Omega}}^2\,\nu}\,\|\mu_H\|_\Lambda\,\|\rho_H\|_\Lambda\,,$$

thus finishing the proof. ∎

Remark 3.2. The fact that the matrix associated to $\mathfrak{B}$ is symmetric positive-definite has multiple advantages from a computational point of view, the possibility of using faster Krylov solvers for its solution being one of them. In addition, it is important to remark that the ellipticity of the bilinear form $\mathfrak{B}$ is independent of ν. Of course, $\mathfrak{B}$ is not defined for $\nu = 0$, but as long as $\nu > 0$, its ellipticity is uniform with respect to it. On the other hand, the lack of uniform stability of T_h with respect to ν is represented by a continuity constant that blows up as $\nu \to 0$. This does not affect the error estimates proven before, as (3.5) is a rewriting of the hybrid formulation (2.17). Nevertheless, for small values of ν the matrix associated to (3.5) may become ill-conditioned as $\nu \to 0$. We will study the extent to which this holds in the numerical experiments in section 4.

Remark 3.3. We finish this section by showing how to implement the MH method solving local problems, thus avoiding a global solution to compute the mappings T_h and $\hat{T}_h$. From (3.3) and (3.4), and thanks to the local definition of the space V_h, we can see that, in each $K \in \mathscr{P}_\mathcal{H}$, $T_h\rho|_K \in V_h(K)$ and $\hat{T}_h f|_K \in V_h(K)$ are the unique solutions of the following local problems:

$$a_K(T_h\,\rho\,, v_h) = -\,\langle \rho\,, v_h\rangle_{\partial K}\,,\ \text{ for all } v_h \in V_h(K)\,, \tag{3.12}$$

$$a_K(\hat{T}_h\,f\,, v_h) = (f, v_h)_K\,,\ \text{ for all } v_h \in V_h(K)\,, \tag{3.13}$$

where the local bilinear form $a_K(\cdot,\cdot)$ is given by

$$a_K(u\,, v) := (\mathcal{K}\,\nabla u, \nabla v)_K + \langle (u\boldsymbol{\sigma})\cdot \boldsymbol{n}^K\,, v\rangle_{\partial K}\,. \tag{3.14}$$

Problems (3.12) and (3.13) are well-posed. In fact, following exactly the same steps as in the proof of Theorem 2.2, we can see that the following holds

$$a_K(v,v) \geq \frac{1}{2}\,\left(\|\mathcal{K}^{\frac{1}{2}}\nabla v\|_{0,K}^2 + \nu\,\|v\|_{0,K}^2\right)\,,\ \text{for all } v \in H^1(K)\,. \tag{3.15}$$

3.1. The MH-Algorithm. The decomposition of (3.3) into the local problems (3.12), coupled with an appropriate selection of basis for Λ_H, provides an *embarrassingly parallel* process to compute the basis functions in the MH method (3.5). More precisely, if $\{\psi_1,\ldots,\psi_N\}$ is a basis for Λ_H, then we start by rewriting it in the following way

$$\{\psi_1,\ldots,\psi_N\} = \bigcup_{F\in\mathcal{E}_H}\,\left\{\phi_1^F,\ldots\phi_{\ell+1}^F\right\}\,, \tag{3.16}$$

where each $\phi_1^F,\ldots,\phi_{\ell+1}^F$ has support in each $F \in \mathcal{E}$. To give a concrete definition of ϕ_j^F for each $j = 1\ldots,\ell+1$, we shall fix a basis $\{\varphi_1,\ldots,\varphi_{\ell+1}\}$ for $\mathbb{P}_\ell(F)$, then we

define $\phi_j^F = (\boldsymbol{n}^F \cdot \boldsymbol{n}_F^K)\,\varphi_j$ for all $j = 1, \ldots, \ell+1$, i.e. if $K_1^F, K_2^F \in \mathscr{P}_{\mathcal{H}}$ are such that $F = K_1^F \cap K_2^F$ and $K_1^F \neq K_2^F$, then $\phi_j^F|_{\partial K_1^F} = -\,\phi_j^F|_{\partial K_2^F}$. Definition (3.16) induces the existence of a global-local bijection $\psi_i \leftrightarrow \phi_k^F$, i.e., it is possible to build a transformation from local to global indexes, denoted by

$$(k, F) \mapsto i(k, F)\,, \tag{3.17}$$

where we have abused the notation using F instead of the index of F in some data structure associated to the mesh $\mathcal{E}_H$. Using (3.16) we rewrite the global problem (3.5) as the linear system: *Find* $(c_1, \ldots, c_N) \in \mathbb{R}^N$ *such that*

$$-\begin{pmatrix} \langle \psi_1\,, T_h\,\psi_1\rangle_{\partial\mathscr{P}_{\mathcal{H}}} & \cdots & \langle \psi_1\,, T_h\,\psi_N\rangle_{\partial\mathscr{P}_{\mathcal{H}}} \\ \vdots & \ddots & \vdots \\ \langle \psi_N\,, T_h\,\psi_1\rangle_{\partial\mathscr{P}_{\mathcal{H}}} & \cdots & \langle \psi_N\,, T_h\,\psi_N\rangle_{\partial\mathscr{P}_{\mathcal{H}}} \end{pmatrix} \begin{pmatrix} c_1 \\ \vdots \\ c_N \end{pmatrix} = \begin{pmatrix} \langle \psi_1\,, \hat{T}_h\,f\rangle_{\partial\mathscr{P}_{\mathcal{H}}} \\ \vdots \\ \langle \psi_N\,, \hat{T}_h\,f\rangle_{\partial\mathscr{P}_{\mathcal{H}}} \end{pmatrix}. \tag{3.18}$$

So, (3.2) can be rewritten as

$$u_h = \sum_{i=1}^{N} c_i\,T_h\,\psi_i + \hat{T}_h\,f\,. \tag{3.19}$$

Now, we will briefly analyse how to compute the entries $\langle \psi_j\,, T_h\,\psi_i\rangle_{\partial\mathscr{P}_{\mathcal{H}}}$. As ψ_j is an element of the basis (3.16), its support is a subset of exactly one $F \in \mathcal{E}_H$. This element F is shared by at most two polygons $\{K_1^F, K_2^F\} := \mathscr{P}_H^F \subseteq \mathscr{P}_{\mathcal{H}}$. Following a close construction we associate to ψ_i two polygons $\{K_1^{F'}, K_2^{F'}\} := \mathscr{P}_H^E \subseteq \mathscr{P}_{\mathcal{H}}$ with $F' \in \mathcal{E}_H$. Using this writing we obtain

$$\langle \psi_j\,, T_h\,\psi_i\rangle_{\partial\mathscr{P}_{\mathcal{H}}} = \sum_{K \in \mathscr{P}_H^F \cap \mathscr{P}_H^E} \langle \psi_j\,, T_h\,\psi_i\rangle_{\partial K} = \sum_{K \in \mathscr{P}_H^F \cap \mathscr{P}_H^E} \int_F \psi_j\,T_h\,\psi_i\,. \tag{3.20}$$

So, the sum above may be zero (when $\mathscr{P}_H^F \cap \mathscr{P}_H^E = \emptyset$), have only one term (when the edge F is on the boundary of Ω) or be composed by two terms. Just as in a classical finite element method implementation, we propose to approach (3.20) through contributions element-by-element with respect to the partition $\mathscr{P}_{\mathcal{H}}$, i.e., for each $K \in \mathscr{P}_{\mathcal{H}}$, $F, F' \subset \partial K$, $k, m \in \{1, \ldots, \ell+1\}$:

$$\int_F \phi_k\,T_h\,\phi_m \xmapsto{\text{contributes to}} \langle \psi_{i(k,F)}\,, T_h\,\psi_{i(m,F')}\rangle_{\partial\mathscr{P}_{\mathcal{H}}} \tag{3.21}$$

where the mapping $i : \mathbb{N} \times \mathbb{N} \to \mathbb{N}$ was introduced in (3.17). Similarly, we notice that

$$\int_F \phi_k\,\hat{T}_h\,f \xmapsto{\text{contributes to}} \langle \psi_{i(k,F)}\,, \hat{T}_h\,f\rangle_{\partial\mathscr{P}_{\mathcal{H}}}\,. \tag{3.22}$$

The only part left to be explained in the MH algorithm is how the terms $T_h\phi_m$ and $\hat{T}_h f$ are computed on each $K \in \mathscr{P}_{\mathcal{H}}$. Let $\{\xi_1, \ldots, \xi_{N_K}\}$ be a basis for $V_h(K)$. From the discrete variational problems (3.3) we see that $T_h\psi_i$ can be written as $T_h\psi_i = \sum_{k=1}^{N_K} t_k^{(i)}\,\xi_k$, where $(t_1^{(i)}, \ldots, t_{N_K}^{(i)}) \in \mathbb{R}^{N_K}$ solves the following linear system:

$$\begin{pmatrix} a_K(\xi_1, \xi_1) & \cdots & a_K(\xi_{N_K}, \xi_1) \\ \vdots & \ddots & \vdots \\ a_K(\xi_1, \xi_{N_K}) & \cdots & a_K(\xi_{N_K}, \xi_{N_K}) \end{pmatrix} \begin{pmatrix} t_1^{(i)} \\ \vdots \\ t_{N_K}^{(i)} \end{pmatrix} = -\begin{pmatrix} \int_F \psi_i\,\xi_1 \\ \vdots \\ \int_F \psi_i\,\xi_{N_K} \end{pmatrix}, \tag{3.23}$$

where $F \in \mathcal{E}_H$ is the only element containing the support of ψ_i. Similarly, from (3.4) we obtain $\hat{T}_h f|_{K_n} = \sum_{k=1}^{N_K} f_k \, \xi_k$ by solving

$$\begin{pmatrix} a_K(\xi_1,\xi_1) & \cdots & a_K(\xi_{N_K},\xi_1) \\ \vdots & \ddots & \vdots \\ a_K(\xi_1,\xi_{N_K}) & \cdots & a_K(\xi_{N_K},\xi_{N_K}) \end{pmatrix} \begin{pmatrix} f_1 \\ \vdots \\ f_{N_K} \end{pmatrix} = \begin{pmatrix} (f\,,\xi_1)_K \\ \vdots \\ (f\,,\xi_{N_{K_n}})_K \end{pmatrix}. \tag{3.24}$$

Finally, we notice that after solving the linear systems (3.23) and (3.24), the right hand side of (3.23) provides an easy way to compute the contributions (3.21) and (3.22) to assemble (3.18) through the following matrix-vector products

$$\int_F \psi_i \, T_h \, \psi_j = \sum_{k=1}^{N_K} t_k^{(j)} \int_F \psi_i \, \xi_k \,, \text{ and, } \int_F \psi_i \, \hat{T}_h f = \sum_{k=1}^{N_K} f_k \int_F \psi_i \, \xi_k \,. \tag{3.25}$$

Algorithm 3.1 summarizes the main steps explained above to compute an MH solution.

Algorithm 3.1 Compute an MH solution.

parfor $K \in \mathscr{P}_{\mathcal{H}}$ **do**
  Assemble the left-hand side $\mathbb{A}$ of (3.23);
  Assemble the right-hand side $\boldsymbol{b}_f$ of (3.24);
  parfor $F \in \partial K$ **do**
    parfor $j = 1, \ldots, \ell + 1$ **do**
      Assemble the j-th column of the right-hand side $\mathbb{B}_K(:, j)$ of (3.23);
    end parfor
  end parfor
  Solve $\mathbb{A} * [\mathbb{E}_K \;\; \boldsymbol{f}_K] = [\mathbb{B}_K \;\; \boldsymbol{b}_f]$; (see (3.23) and (3.24))
  $-\mathbb{E}_K^T * \mathbb{B}_K \xmapsto{\textit{contributes to}} \mathbb{M}$; (left-hand side of (3.18), see also (3.21) and (3.25))
  $\boldsymbol{f}_K^T * \mathbb{B}_K \xmapsto{\textit{contributes to}} \boldsymbol{L}$; (right-hand side of (3.18), see also (3.22) and (3.25))
end parfor
Solve $\mathbb{M} * \boldsymbol{V} = \boldsymbol{L}$;
parfor $K \in \mathscr{P}_{\mathcal{H}}$ **do**
  Extract $\boldsymbol{V}_K$ from $\boldsymbol{V}$; (coefficients related to K)
  $\boldsymbol{u}_K = \boldsymbol{V}_K^T * \mathbb{E}_K + \boldsymbol{f}_K$; (see (3.19))
end parfor

4. Computational Experiments. In this section we set the unit square, $\Omega = (0,1)^2$, as the domain of problem (1.1). We will present four series of numerical experiments showcasing the performance of the method from different points of view. To avoid any pollution from the solution of the local problems, we have always taken $k = \ell + 2$. So, the convergence will always be measured with respect to the order of approximation in Λ_H, namely ℓ.

4.1. Convergence Assessment. We first test the convergence of the method for a problem with smooth data and solutions. We consider $\mathcal{K} = \mathcal{I}$ and

$$f(x,y) = 4\,(n^2 + m^2)\,\pi^2 \, \sin(2\,n\,\pi\,x) \, \sin(2\,m\,\pi\,y)\,, \text{ in } \Omega\,,$$

with $n, m \in \mathbb{N}$. So, the exact solution of (1.1) is given by

$$u(x,y) = \sin(2\,n\,\pi\,x) \, \sin(2\,m\,\pi\,y)\,. \tag{4.1}$$

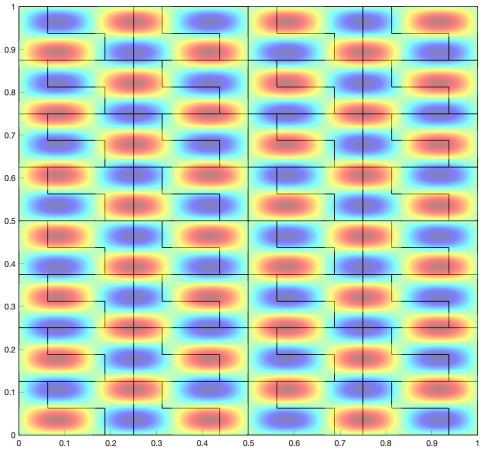

FIG. 2. *Example of approximated solution obtained with the MH method on a mesh composed by L-shaped polygons. The shortest edge in each polygon has size* $\frac{1}{16}$ *and the longest has size* $\frac{1}{8}$*. The computational edges in* $\mathcal{E}_H$ *have size* $H = \frac{1}{64}$*. In addition,* $h = \frac{1}{1024}$*,* $\ell = 1$*, and* $k = 3$*.*

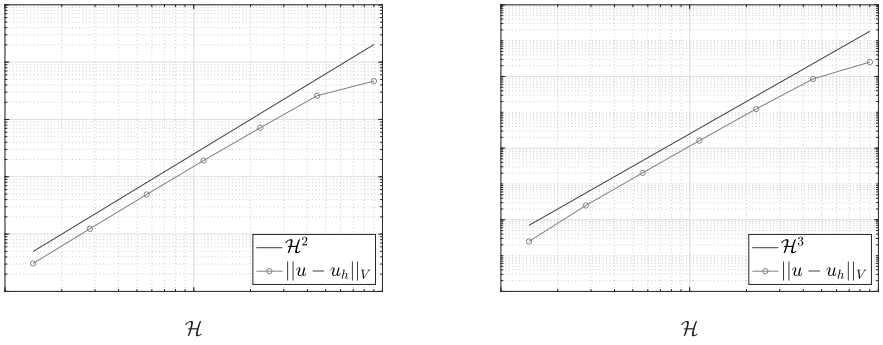

FIG. 3. *Mesh based convergence for* $\nu = \frac{1}{4}$ *and* $H = \mathcal{H}$ *. Here it was used* $\ell = 1$ *and* $k = 3$ *(left) and* $\ell = 2$ *and* $k = 4$ *(right). The second level was computed with* $h = \frac{1}{256}$*.*

In the convergence results presented below we set $n = 3$ and $m = 7$ in the exact solution (4.1).

The first convergence test is carried out on a family of partitions composed by L-shaped polygons. In Figure 2 we depict the discrete solution for one particular mesh in the family, using $H = \frac{1}{64}$ and $h = \frac{1}{1024}$. Thanks to our choice $k = \ell + 2$ and the small value $h = \frac{1}{256}$, both chosen to avoid any pollution arising from the second level calculations on the convergence, Corollary 2.7 predicts an $O(\mathcal{H}^{\ell+1})$ convergence rate. The results shown in Figure 3 reflect this optimal convergence rate both for $\ell = 1, k = 3$ (left panel) and $\ell = 2, k = 4$ (right panel). For this first experiment, the value ν has been chosen equal to $\frac{1}{4}$, and the skeleton mesh $\mathcal{E}_H$ coincides with $\mathcal{E}$, i.e. $H = \mathcal{H}$.

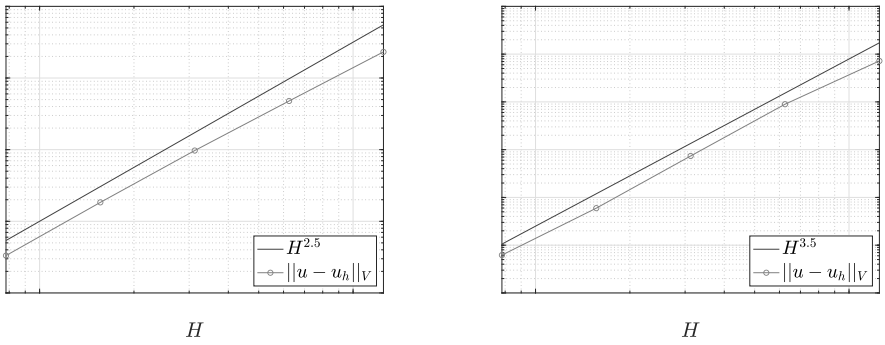

FIG. 4. *Space based convergence for* $\mathcal{H} = \frac{1}{4}\sqrt{13}$ *and* $\nu = \frac{1}{4}$. *The second level was computed with* $h = \frac{1}{256}$. *The error curves on the left side were made for* $\ell = 1$ *and* $k = 3$, *whereas on the right side we present curves for for* $\ell = 2$ *and* $k = 4$.

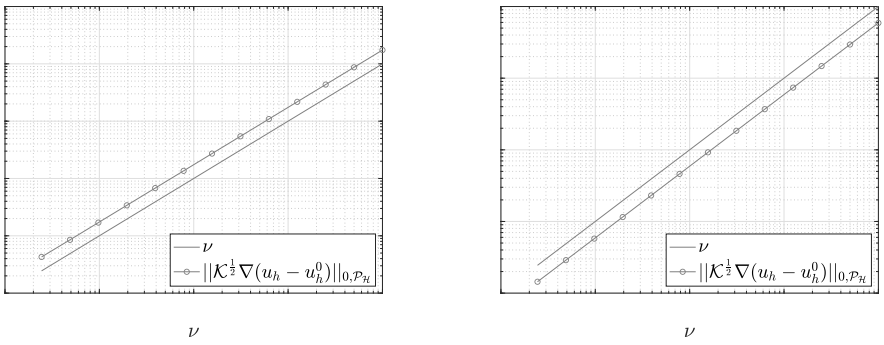

FIG. 5. *Difference between the MH and MHM solutions as* $\nu \to 0$. *On the left panel we use a mesh using squares of size* $\mathcal{H} = \frac{1}{8}$, *with* $\ell = 1$, $k = 3$, $h = \frac{1}{8}\mathcal{H}$, $H = \frac{1}{4}\mathcal{H}$. *On the right panel we used a criss-cross mesh composed by triangles with* $\mathcal{H} = \frac{1}{4}$, $\ell = 2$, $k = 4$, $h = \frac{1}{16}\mathcal{H}$, $H = \mathcal{H}$.

We next study the convergence behavior on H by fixing the partition $\mathscr{P}_\mathcal{H}$ as the mesh presented in Figure 2 and making successive refinements on $\mathcal{E}_H$ (referred to as *space-based* convergence in [8]). The value $h = \frac{1}{256}$ is sufficiently small as to ensure that the second level calculations do not polute the errors. The results presented in Figure 4 show a *super-convergence* with respect to the theoretical estimate given by Corollary 2.7. More precisely, both rates are one half higher than expected. Such behavior was observed in the MHM method in [8] and has been recently analyzed in [11].

Finally, we test the convergences presented in Theorem 2.10. For this, we use two types of meshes. More precisely, we consider two fixed partitions $\mathscr{P}_\mathcal{H}$, one composed of triangles and the other one of squares (see Figure 5 for details). In Figure 5 we report the evolution of the error $\|\mathcal{K}^{\frac{1}{2}}\nabla(u_h - u_h^0)\|_{0,\mathscr{P}_\mathcal{H}}$, where we see that, as predicted by Theorem 2.10, the decrease in the error is linear, thus confirming that the solution of the MH method does approach that of the MHM method as $\nu \to 0$.

4.2. Conditioning with respect to ν and its numerical consequences. In section 3 we analyzed the stability of local and global problems, (3.3)-(3.4) and (3.5), respectively. This analysis reveals that the ellipticity of the local problems depends strongly on ν, and that the norm of the bilinear form associated to the global problem grows up as ν^{-1} when $\nu \to 0$. In this section we validate those claims numerically by computing the largest and smallest singular values of the respective matrices obtained by approximating the solution to the problem described in subsection 4.1 with $n = 3$ and $m = 7$ and using the space settings detailed in Figure 6. We depict the obtained results in Figure 6, along with the same quantities obtained for the MHM method (the latter is added for reference, as the MHM method does not involve ν).

The results depicted in Figure 6 show that the MH method indeed produces matrices whose condition number is worse than those of the MHM method (the ellipticity constants are slightly better than those of the MHM method, but the continuity ones clearly blow up with ν^{-1}, reproducing the fact that the MH method is not defined for $\nu = 0$). These results raise the question about the influence of the value of ν in the quality of the results provided by the MH method. From a theoretical point of view, the answer is clear. As a matter of fact, the convergence rates presented in Corollary 2.7 are not affected by the value of ν. This implies, in particular, that the solution obtained by the MH algorithm (i.e., the function u_h computed using (3.2)) converges to the exact solution with rates (and values) that are independent of ν. However, from a practical point of view, the degeneration of the condition number can affect the quality of the approximate solution to a discrete problem. To make a finer assessment on this situation, in Figure 8 we present the convergence curves for different choices of ν. The results depicted in that figure show that the rates (and values) of the error are virtually unaffected with values of ν larger than, or equal to, 6×10^{-8}. When ν reaches that value, the condition number of the local and global problems start getting affected by the value of ν, and this can affect the overall quality of the solution, as can be concluded from the error curve depicted using $\nu = 3.7 \times 10^{-9}$.

To complement the above discussion, in Figure 9 we depict the error of the MH method for a range of values of ν, and also report the error obtained when solving the exact same problem with the MHM method. From those results we observe that for a moderate range of ν, that is, for ν ranging from 10^{-8} to 1, the error of the MH method is similar or slightly smaller than that of the MHM method, while for smaller values of ν the quality of the solution of the MH method deteriorates.

To summarize the above discussion, in our experience it is safe to use the MH method for values of ν that are not smaller than 10^{-6}.

4.3. Capture of Multiscale Features. In this section we showcase the capabilities of the presented method for two problems with highly oscillating coefficients that are not resolved by the mesh $\mathscr{P}_{\mathcal{H}}$.

4.3.1. A highly-oscillatory problem. We first approximate the solution to (1.1) with a non-homogenous dirichlet boundary condition $u|_{\partial\Omega} = g$ and assuming a highly-oscillatory data of periodicity $\varepsilon > 0$ for (1.1). More precisely, we consider the following data

$$\begin{aligned}
\mathcal{K}(x,y) &= \left(\frac{17}{16} + \cos\left(\frac{\pi}{\varepsilon}\,x\right)\,\sin\left(\frac{\pi}{2\,\varepsilon}\,x\right)\right)\,\mathrm{I}_2\,,\\
f(x,y) &= \sin(x)\,\sin(y) + \cos\left(\frac{\pi}{17\,\varepsilon}\,x\right)\,\sin\left(\frac{\pi}{23\,\varepsilon}\,x\right)\,,\\
g(x,y) &= 10^{-2}\,\cos(3\,\pi\,x)\,\cos(5\,\pi\,y)\,,
\end{aligned}$$

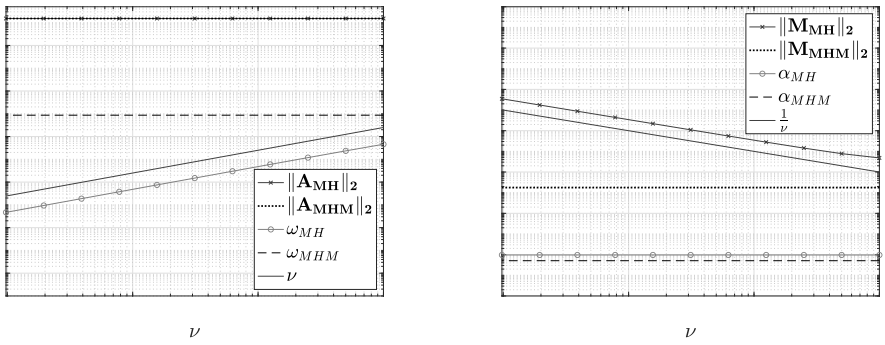

FIG. 6. *Behaviour of ellipticity constants and norms for local (left) and global (right) systems for the presented method compared with same quantities obtained for the MHM method. The used configuration was* $\ell = 1$, $H = \frac{\mathcal{H}}{4}$, $h = \frac{\mathcal{H}}{8}$, *and,* $k = 3$, *with* $\mathcal{H} = \frac{1}{8}$, *on a criss-cross mesh.*

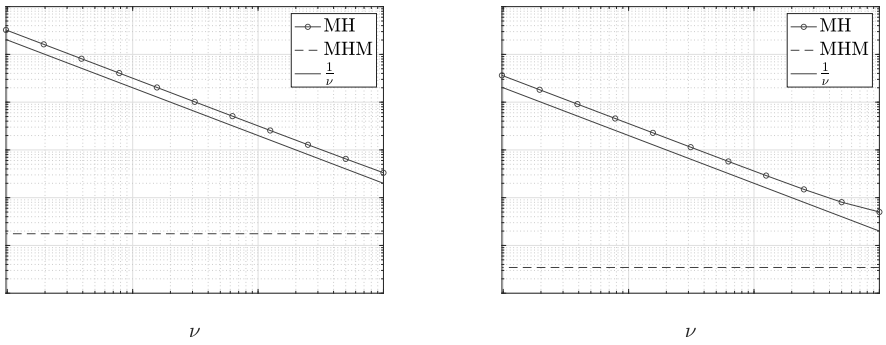

FIG. 7. *Condition Numbers of the local (left) and global (right) linear varying with respect to* ν *for the presented method compared with same quantities obtained for the MHM method. The used configuration was* $\ell = 1$, $H = \frac{\mathcal{H}}{4}$, $h = \frac{\mathcal{H}}{8}$, *and,* $k = 3$, *with* $\mathcal{H} = \frac{1}{8}$, *on a criss-cross mesh.*

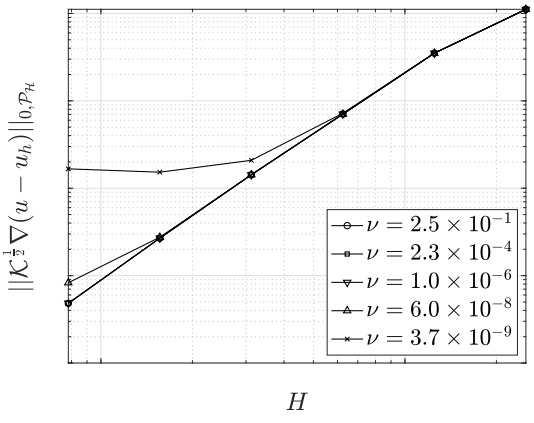

FIG. 8. *Influence of* ν *on the convergence rates with respect to* H. *Here it was used* $\ell = 1$, $k = 3$, $h = \frac{1}{64}\mathcal{H}$, *and,* $\mathcal{H} = \frac{1}{4}$, *on a criss-cross mesh.*

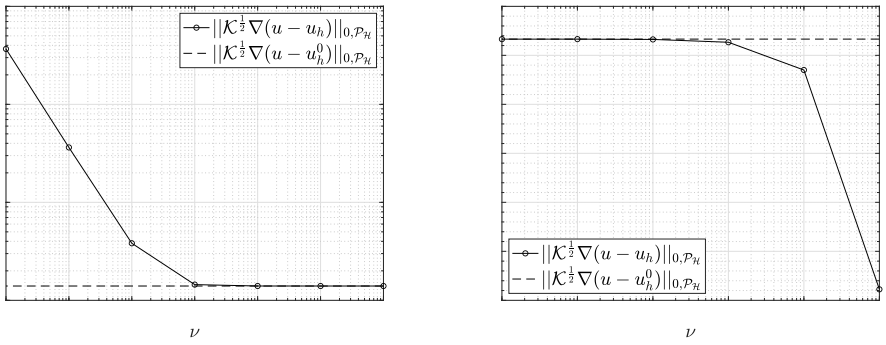

FIG. 9. *Two regimes for the behaviour of the error obtained for the presented method compared with the error of the MHM method: Small (left) and large (right) values of ν. The used configuration was $\ell = 1$, $k = 3$, $h = \frac{\mathcal{H}}{16}$, and, $H = \frac{\mathcal{H}}{8}$, with $\mathcal{H} = \frac{1}{4}$, on a criss-cross mesh.*

defined for all $(x, y) \in \Omega$. We consider $\varepsilon = \frac{1}{337}$, and compute a reference solution using the Galerkin method with $\mathbb{Q}_3$ elements in a highly refined mesh containing 4,194,304 uniform quadrilateral elements. Figure 10 depicts the reference solution, where we can observe its highly oscillating character due to the definition of $\mathcal{K}$. We observe that the method (3.5) needs to be sightly modified as follows to treat non-homogeneous boundary conditions: Find $\lambda_H \in \Lambda_H$ such that

$$\mathfrak{B}(\lambda_H, \mu_H) = \langle \mu_H \, , \hat{T}_h \, f \rangle_{\partial \mathscr{P}_\mathcal{H}} - \langle \mu_H \, , g \rangle_{H^{-\frac{1}{2}}(\partial\Omega), H^{\frac{1}{2}}(\partial\Omega)} \, , \text{ for all } \mu_H \in \Lambda_H \, , \tag{4.2}$$

where we assumed that $g \in H^{\frac{1}{2}}(\partial\Omega)$. Then, we compute the MH approximation through (4.2) in a mesh containing 64 square elements, i.e., $\mathcal{H} = \frac{1}{8}\sqrt{2}$, with spaces Λ_H and V_h using $\ell = 1$, $k = 3$, $h = \frac{1}{256}\,\mathcal{H}$, and, $H = \frac{1}{8\sqrt{2}}\,\mathcal{H}$. The MH solution is depicted in Figure 11 where we can observe a good agreement between the MH solution and the reference. In Figure 12 we depict the error between the MH solution and the reference one as $H \to 0$. For this we have used a space-based approach (so, keeping $\mathcal{H}$ fixed). We can observe in the left panel that the error decreases with the expected rate $O(H^2)$. In addition, on the right panel of Figure 12 we depict the error for the largest value of H and a range of values of ν where we can observe that the error is very robust with respect to the value of ν.

4.3.2. A porous media fluid flow problem. Now, we conduct an experiment inspired by [35], which lies outside the theory presented in the current work. However, we find it valuable to demonstrate the potential applications of our approach. Specifically, we modify the problem by introducing a subset of the boundary denoted as $\Gamma_N \subseteq \partial\Omega$. We alter the original elliptic equation (1.1) to include boundary conditions: $u|_{\partial\Omega\setminus\Gamma_N} = g$ and $-\mathcal{K}\nabla u \cdot \boldsymbol{n}|_{\Gamma_N} = 0$, where $\boldsymbol{n}$ represents the outward normal vector to Ω. This induces a slight modification of the method as the facets on Γ_N are no longer needed in its construction. This resulting variant can also be analyzed with arguments related to the ones presented herein. We will omit the details to avoid technical diversions, and for brevity.

Let consider the domain $\Omega = (0, 1.2\times10^3)\times(0, 2.2\times10^3)$ with $\Gamma_N = \{(x, y) \in \partial\Omega : (x = 0),$ or, $(x = 1.2 \times 10^3)\}$ and define the permeability $\mathcal{K}$ based on the 36^{th} layer of Model 2 from the 10th Comparative Solution Project conducted by the Society

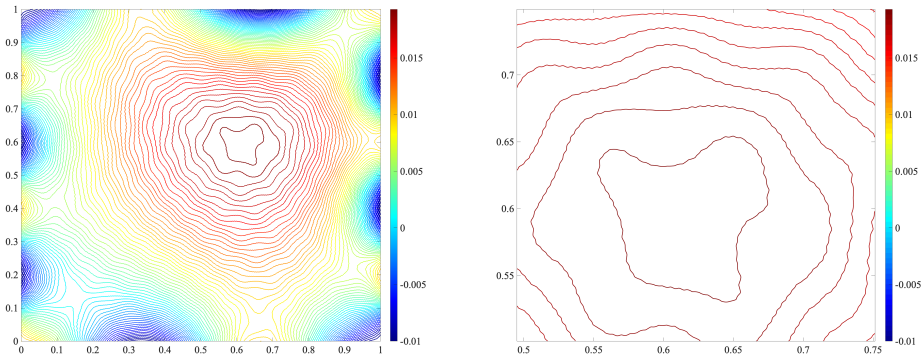

FIG. 10. *Reference solution computed wtih the classical Galerkin method using $\mathbb{Q}_3$ elements on a square mesh with 4,194,304 elements and 37,736,449 degrees of freedom. Levelset curves (left) and zoom around $\left(\frac{5}{8}, \frac{5}{8}\right)$ (right).*

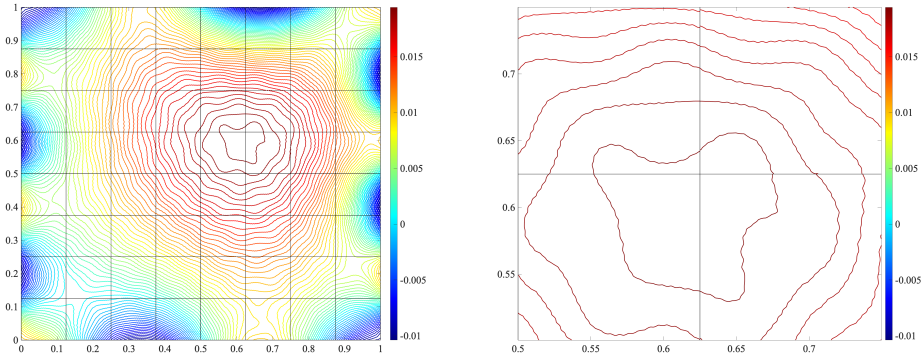

FIG. 11. *At left levelset curves of the approximated solution computed by the MH method for $\varepsilon = \frac{1}{337}$. Here, $\ell = 1$, $k = 3$, $h = \frac{1}{256}\,\mathcal{H}$, $H = \frac{1}{8}\,\frac{\mathcal{H}}{\sqrt{2}} = \frac{1}{64}$, with $\mathcal{H} = \frac{1}{8}\sqrt{2}$, on a mesh composed by 64 squares. At right zoom around $\left(\frac{5}{8}, \frac{5}{8}\right)$.*

of Petroleum Engineers (SPE10) [33]. For this problem $\mathcal{K}(x, y) = \kappa(x, y)\,\mathrm{I}_2$, for all $(x, y) \in \Omega$, where $\kappa(x, y)$ is depicted in Figure 13. This definition serves as the basis for validating the MH method with $\ell = 1$ on the faces of a quadrilateral mesh comprising 66 squares. The model problem includes an imposed entry pressure of 1 at the bottom side and 0 at the top, i.e., $g(x, y) = 1 - \frac{1}{2.2\times 10^3}\,y$, for all $(x, y) \in \partial\Omega\backslash\Gamma_N$. As mentioned above, homogeneous Neumann conditions are applied to the other two boundaries, while the source term is $f = 0$. It is worth mentioning that we employ a reference solution (refer to Figure 13) generated using continuous $\mathbb{Q}_3$ elements in a quadrilateral mesh consisting of 1,081,344 elements, corresponding to 9,738,625 degrees of freedom. In Figure 14 we depict the MH solution (obtained using $\nu = 10^{-4}$) and the reference one. We can observe a very good agreement between the two solutions, despite the difference both in number of elements, and degree of approximation. To accentuate

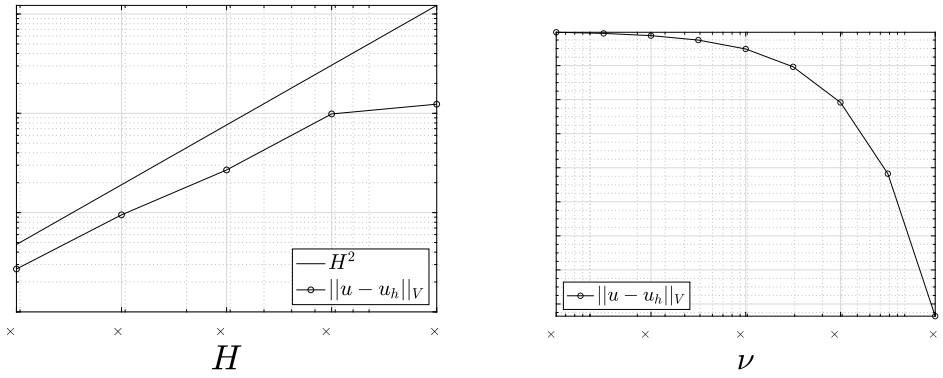

FIG. 12. *Convergence on H with respect to the reference (left) and influence of ν on the approximation error for the MH method (right). Here it was used $\ell = 1$, $k = 3$, $h = \frac{1}{64}\mathcal{H}$, with $\mathcal{H} = \frac{1}{8}\sqrt{2}$ on a mesh composed by squares.*

this similarity further, we present cross-sectional profiles of both solutions at $x = 199$ in Figure 15. These profiles reveal a strong agreement between the reference solution and the MH approximation, achieved by subdividing each edge into eight segments to define the polynomial interpolation. For a more comprehensive examination of each approximation's behavior, we offer an enlarged view of Figure 15 in Figure 16.

4.4. Performance Analysis. In this section we compare the computational performance of the MH method with that of the MHM method presented in [8]. Both methods were used for solving problem (1.1) with the same Ω, $\mathcal{K}$ and f used in subsection 4.1 (see Figure 17 for details about the meshes and polynomial degrees used). The simulations were conducted using a C++ framework developed in-house for implementing finite-element solvers.[1] The framework implements the MH and MHM methods, and also the classical Galerkin method used for solving the local problems of both multiscale methods. The framework allows for multithreaded, shared memory parallelism using OpenMP, and multiprocessing, distributed memory parallelism using MPI. The framework is linked to two main libraries: (i) Eigen [21], for general matricial operations and also for solving the linear systems generated by the local problems; and (ii) MUMPS [2], for solving the linear system generated by the global problem.

For the experiments conducted in this paper, we used a high-performance cluster. Each node in this cluster has 2 CPUs of 24 cores each and 768 Gb of RAM memory. We considered three simulation configurations: running on a single node, on two nodes, and on four nodes. The computing system is configured so that each MPI process occupies a single CPU; therefore, our simulations run with 2, 4 and 8 MPI processes.

For each simulation, the local problems are uniformly partitioned between the MPI processes. Within each of these processes, the "**parfor**" loops shown in Algorithm 3.1 are implemented with OpenMP so that the local problems pertaining to an MPI process are solved in an embarrassingly parallel way using all the available 24 cores in its CPU. Only the assembly of $\mathbb{M}$ and $\boldsymbol{L}$, and the solution of $\mathbb{M} * \boldsymbol{V} = \boldsymbol{L}$

[1] The code used for this performance analysis and some other experiments presented in this paper is freely available under request at https://gitlab.com/ipes/msl_kernelfreediffusion.

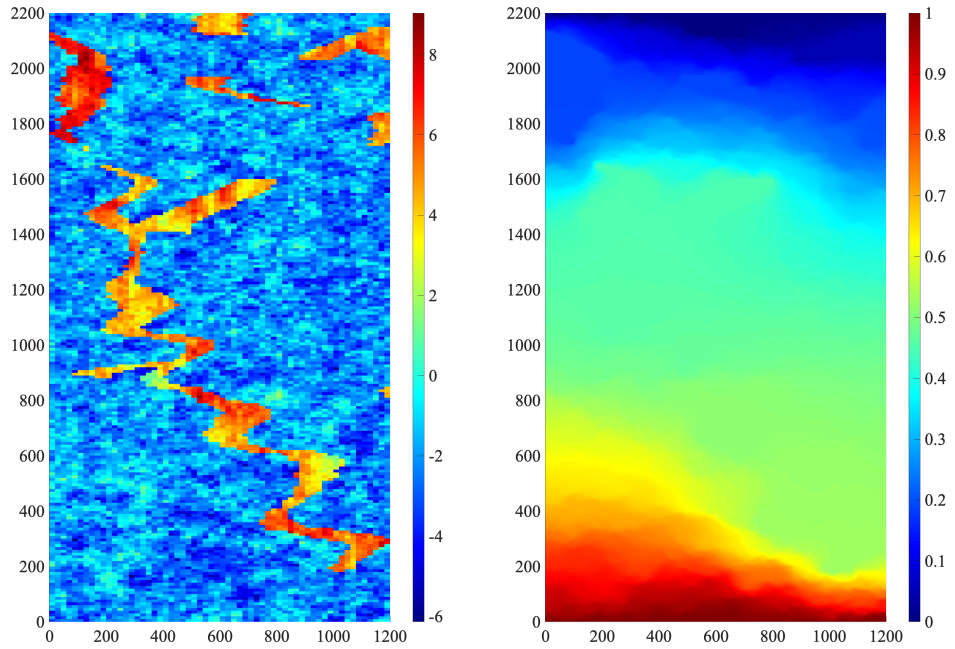

FIG. 13. *Logarithm of the permeability proposed in [33] (left) and the isolvalues of the reference solution (right).*

in Algorithm 3.1 employ tightly-coupled parallelism through MPI messages within the MUMPS library.

In the simulations with MHM, the LU factorization implementations of Eigen (for local problems) and MUMPS (for the global problem) are used. For the implementation of the current MH method, the symmetric positive-definite character of the local and global problems allows us to use the Choleski factorization implementations of Eigen (for local problems) and MUMPS (for the global problem).

The performance metrics used for the comparison between MH and MHM are: (i) the time to assemble and solve all local problems; (ii) the time to assemble and solve the global problem; and (iii) the maximum memory (resident set size – RSS) consumed by the most demanding MPI process in each simulation.

We start describing the case $\ell = 0$. The results depicted in Figure 17 show that, as H decreases, the performance difference in terms of time needed to solve the global problem increases in favour of the MH method. Regarding memory consumption, the MHM method presents better performance for smaller values of H, but this situation changes very early in the refinement process. In fact, when $H \approx 2.44 \times 10^{-4}$ the MHM method is already more memory consuming than the MH method.

To perform the same comparison for higher order elements, in Figure 18 we depict the memory consumption for both the present MH and the MHM methods. From that figure it is clear that the MH method requires considerable less memory than the MHM method, both for $\ell = 1$ and $\ell = 2$. In fact, for $H \approx 2.44 \times 10^{-4}$ the MHM

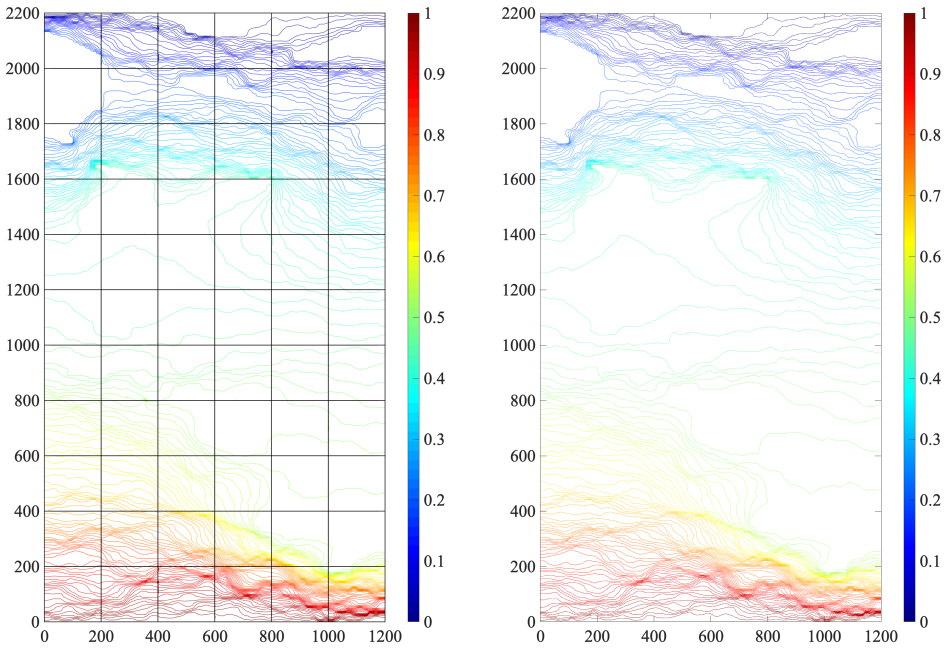

FIG. 14. *Levelset curves of pressure from the MH method with the overlaid quadrilateral mesh composed by 66 squares (left) and the reference solution (right). Here* $\ell = 1$, $h = \frac{1}{64}\mathcal{H}$, *and,* $H = \frac{1}{32\sqrt{2}}\mathcal{H}$.

method could not be solved in 4 cluster nodes due to the lack of memory resources.

The last results were related to the solution of the whole problem, including both the online solution of the global problem, as well as the offline solution of the local ones. We now will take a closer look at the second ingredient. More precisely, we place ourselves in the setting described in Figure 19, and measure the impact of the degree k used to solving the local problems both in the MH and the MHM methods. To achieve that, we have measured the time needed to solve all local problems in both methods. Interestingly, for lower values of k the local problems in the MHM method take slightly less time than those associated to the MH method. This can be explained as follows: the local problems for the MH method are symmetric and elliptic (as opposed to those of the MHM method that are indefinite), but they require to assemble the term $\langle (\boldsymbol{\sigma} \cdot \boldsymbol{n}^K)\ u_h, v_h \rangle_{\partial K}$ as well, which takes some more time. Now, once the polynomial degree k gets high, the symmetry and ellipticity of the local problems for the MH method starts paying off and as a consequence the total time computing the local problems for the MH method becomes lower than the corresponding time for the MHM method. These results can be seen in detail in Figure 19.

These performance results are indicative that the MH method is particularly adequate for challenging problems that demand more space-based refinement and/or higher-order polynomials. To support this argument, we conducted an additional set of experiments using $n = 128$ and $m = 256$ in the model problem presented

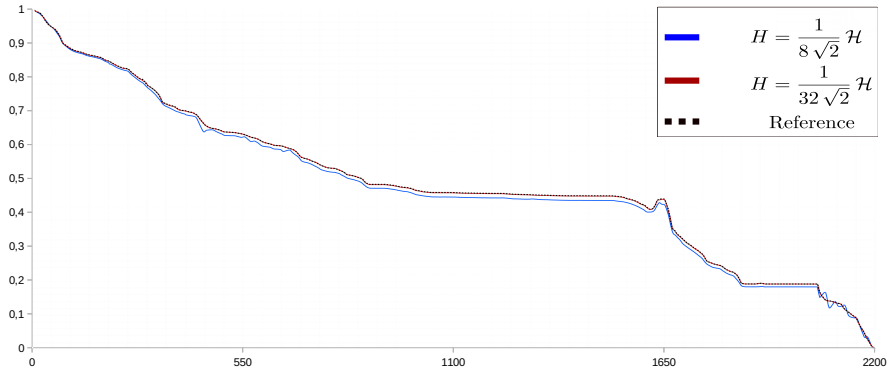

FIG. 15. *Comparison of profiles at* $x = 199$ *of MH approximation with the reference solution. Here,* $\ell = 1$, $k = 3$.

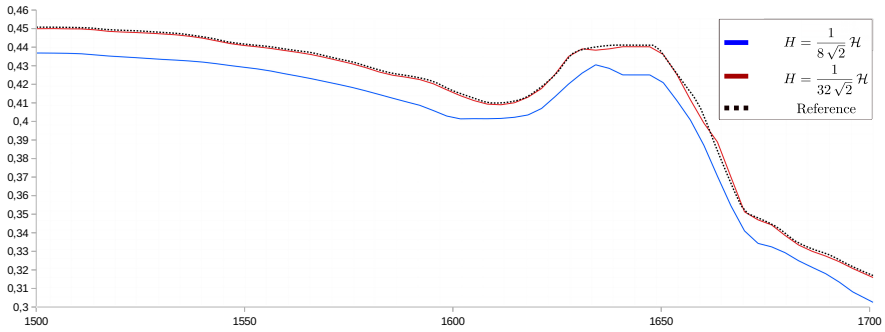

FIG. 16. *Zoom from* $y = 1500$ *to* $y = 1700$ *of the profiles in Figure 15.*

in subsection 4.1, thus we consider the case of a highly oscillatory solution. Figure 20 shows that the MH method considerably reduces the amount of memory needed for reaching the same approximation error as the MHM method in this problem. Again, the MHM simulation could not complete in the most demanding configuration because of the lack of memory resources.

5. Conclusion and outlook. In this work we presented an alternative way to build multiscale methods based on a hybrid formulation. The main advantage of this approach lies on the fact that both the global problem for the discrete Lagrange multipliers, as well as the local problems defining the basis functions, are elliptic. In addition, the approach followed to analyze the error, that is, interpreting the MH method as a reformulation of a hybrid formulation, is, up to our best knowledge, new (and could also be applied to analyze the MHM method itself). Interestingly, the error constants for the MH method are independent of the parameter ν, and also the solution of the MH method was proven to converge to that of the MHM method when $\nu \to 0$. When exploring the performance of the method in this regime, one particular phenomenon emerged, namely, the deterioration of the condition number of the local and global problems for very small values of ν. Thus, our advice to use this scheme with values of ν that are not excessively small.

Several problems remain open at this point. From a theoretical point of view, the

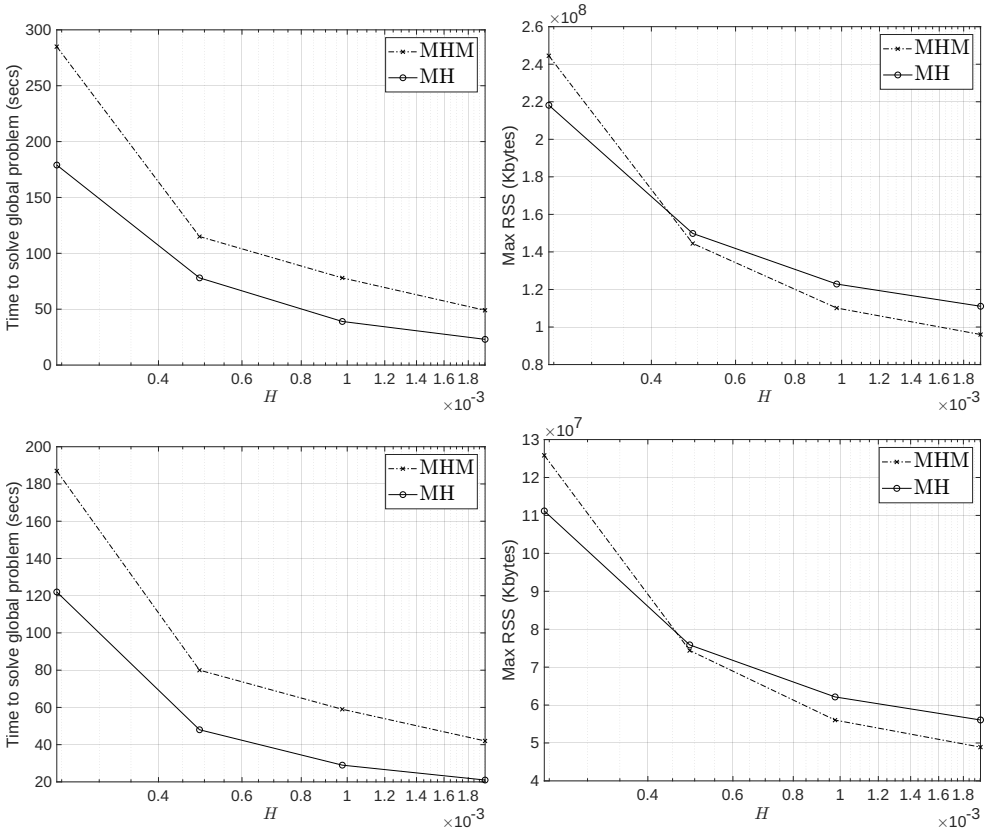

FIG. 17. *Performance results with respect to H. Both the MH and MHM methods used a criss-cross mesh with $\mathcal{H} = \frac{1}{512}$, $\ell = 0$, $k = 2$, and $h = \frac{\mathcal{H}}{16}$. For the MH method, $\nu = \frac{1}{4}$. Left side: Time to compute the global problem. Right side: Maximum RSS of the simulation. Two system configurations were used: 2 MPI processes (top); 4 MPI processes (bottom).*

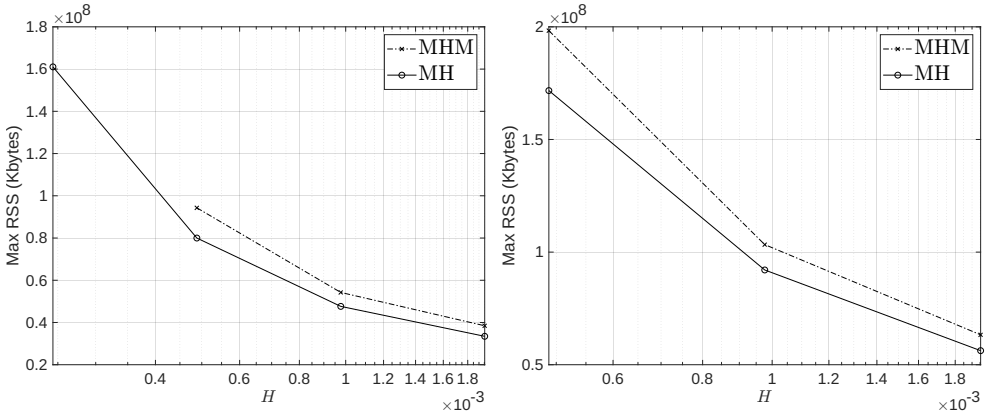

FIG. 18. *Maximum RSS of the simulation with respect to H. Both the MH and MHM methods used a criss-cross mesh with $\mathcal{H} = \frac{1}{512}$ in 8 MPI processes, and were configured with $h = \frac{\mathcal{H}}{16}$. For the MH method, $\nu = \frac{1}{4}$. Left side: $\ell = 1$, $k = 3$. Right side: $\ell = 2$, $k = 4$.*

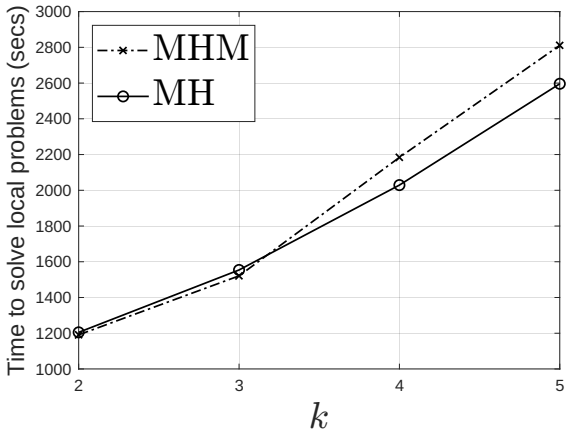

FIG. 19. *Time to solve local problems with respect to k. Both the MH and MHM methods used a criss-cross mesh with $\mathcal{H} = \frac{1}{512}$ in 4 MPI processes, and were configured with $H = \mathcal{H}$, $\ell = k - 2$ and $h = \frac{\mathcal{H}}{16}$. For the MH method, $\nu = \frac{1}{4}$.*

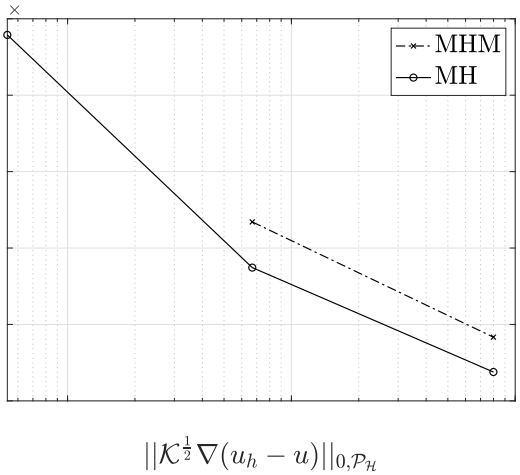

FIG. 20. *Maximum RSS of the simulation with respect to $||\mathcal{K}^{\frac{1}{2}}\nabla(u_h - u)||_{0,\mathcal{P}_\mathcal{H}}$. Both the MH and MHM methods used a criss-cross mesh with $\mathcal{H} = \frac{1}{512}$ in 4 MPI processes, and were configured with $\ell = 2$, $k = 4$ and $h = \frac{\mathcal{H}}{16}$. In both methods, H varied from $\mathcal{H}$ to $\frac{\mathcal{H}}{4}$ to achieve the intended approximation errors. For the MH method, $\nu = \frac{1}{4}$.*

possibility of adapting some of the arguments used in [11] to the present work, thus extending (or making more precise) the error analysis to rough physical coefficients is of interest. In addition, the fact that both the local and global kernels are removed form the formulations can help to adapt the present framework to more involved models, such as the one considered in [12], where geometrical conditions had to be imposed on the mesh and coefficients to be able to deal with the presence of a local kernel. In addition, it is interesting to remark that, even if in practice we use a Robin boundary condition (depending on ν) for the local problems, the control provided by it is not the one we would expect from the use of a Robin condition (cf. the ellipticity in Theorem 2.2). So, a more detailed comparison between the present approach and

others including a more *traditional* Robin condition is also of interest. Finally, from a numerical perspective, the relation between the parameter ν and the condition number of both the local and global problems needs to be studied more in detail, although the restriction that somehow ν needs to be smaller than the smallest eigenvalue of $\mathcal{K}$ needs to be kept in mind. Alternatives to overcome this possible issue, including possibilty the design of appropriate preconditioners for the global problem, also need to be proposed and analyzed. These and other topics are currently underway and will be the subject of future research.

Acknowledgments. The authors acknowledge the National Laboratory for Scientific Computing (LNCC/MCTI, Brazil) for providing HPC resources of the SDumont supercomputer (http://sdumont.lncc.br), which have contributed to the research results reported within this paper.

REFERENCES

[1] R. Altmann, P. Henning, and D. Peterseim, *Numerical homogenization beyond scale separation*, Acta Numerica, 30 (2021), p. 1–86, https://doi.org/10.1017/S0962492921000015.

[2] P. R. Amestoy, I. S. Duff, J. Koster, and J.-Y. L'Excellent, *A fully asynchronous multifrontal solver using distributed dynamic scheduling*, SIAM Journal on Matrix Analysis and Applications, 23 (2001), pp. 15–41.

[3] R. Araya, C. Harder, D. Paredes, and F. Valentin, *Multiscale hybrid-mixed method*, SIAM J. Numer. Anal., 51 (2013), pp. 3505–3531, https://doi.org/10.1137/120888223.

[4] T. Arbogast and K. J. Boyd, *Subgrid upscaling and mixed multiscale finite elements*, SIAM Journal on Numerical Analysis, 44 (2006), pp. 1150–1171, https://doi.org/10.1137/050631811.

[5] T. Arbogast, G. Pencheva, M. F. Wheeler, and I. Yotov, *A multiscale mortar mixed finite element method*, Multiscale Modeling & Simulation, 6 (2007), pp. 319–346, https://doi.org/10.1137/060662587.

[6] I. Babuška and J. E. Osborn, *Generalized finite element methods: their performance and their relation to mixed methods*, SIAM J. Numer. Anal., 20 (1983), pp. 510–536, https://doi.org/10.1137/0720034.

[7] R. E. Bank, A. H. Sherman, and A. Weiser, *Some refinement algorithms and data structures for regular local mesh refinement*, Scientific Computing, Applications of Mathematics and Computing to the Physical Sciences, 1 (1983), pp. 3–17.

[8] G. R. Barrenechea, F. Jaillet, D. Paredes, and F. Valentin, *The multiscale hybrid mixed method in general polygonal meshes*, Numer. Math., 145 (2020), pp. 197–237, https://doi.org/10.1007/s00211-020-01103-5.

[9] S. C. Brenner, *Poincaré-Friedrichs inequalities for piecewise H^1 functions*, SIAM J. Numer. Anal., 41 (2003), pp. 306–324, https://doi.org/10.1137/S0036142902401311.

[10] T. Chaumont-Frelet, A. Ern, S. Lemaire, and F. Valentin, *Bridging the multiscale hybrid-mixed and multiscale hybrid high-order methods*, ESAIM Math. Model. Numer. Anal., 56 (2022), pp. 261–285, https://doi.org/10.1051/m2an/2021082, https://doi.org/10.1051/m2an/2021082.

[11] T. Chaumont-Frelet, D. Paredes, and F. Valentin, *Flux approximation on unfitted meshes and application to multiscale hybrid-mixed methods*. Preprint, Oct. 2022, https://hal.inria.fr/hal-03834748.

[12] T. Chaumont-Frelet and F. Valentin, *A multiscale hybrid-mixed method for the Helmholtz equation in heterogeneous domains*, SIAM J. Numer. Anal., 58 (2020), pp. 1029–1067, https://doi.org/10.1137/19M1255616.

[13] M. Cicuttin, A. Ern, and S. Lemaire, *A hybrid high-order method for highly oscillatory elliptic problems*, Comput. Methods Appl. Math., 19 (2019), pp. 723–748, https://doi.org/10.1515/cmam-2018-0013, https://doi.org/10.1515/cmam-2018-0013.

[14] W. E and B. Engquist, *The Heterognous Multiscale Methods*, Communications in Mathematical Sciences, 1 (2003), pp. 87 – 132.

[15] Y. Efendiev and T. Y. Hou, *Multiscale finite element methods*, vol. 4 of Surveys and Tutorials in the Applied Mathematical Sciences, Springer, New York, 2009. Theory and applications.

[16] Y. R. Efendiev, T. Y. Hou, and X.-H. Wu, *Convergence of a nonconforming multiscale finite element method*, SIAM Journal on Numerical Analysis, 37 (2000), pp. 888–910, https:

//doi.org/10.1137/S0036142997330329.
[17] A. Ern and J.-L. Guermond, *Finite elements I—Approximation and interpolation*, vol. 72 of Texts in Applied Mathematics, Springer, Cham, [2021] ©2021.
[18] A. Ern and J.-L. Guermond, *Finite elements II—Galerkin approximation, elliptic and mixed PDEs*, vol. 73 of Texts in Applied Mathematics, Springer, Cham, [2021] ©2021.
[19] M. J. Gander, *Optimized Schwarz methods*, SIAM J. Numer. Anal., 44 (2006), pp. 699–731, https://doi.org/10.1137/S0036142903425409.
[20] A. T. A. Gomes, W. S. Pereira, and F. Valentin, *The MHM Method for Linear Elasticity on Polytopal Meshes*, IMA Journal of Numerical Analysis, (2022), https://doi.org/10.1093/imanum/drac041.
[21] G. Guennebaud, B. Jacob, et al., *Eigen v3*. http://eigen.tuxfamily.org, 2010.
[22] R. T. Guiraldello, R. F. Ausas, F. S. Sousa, F. Pereira, and G. C. Buscaglia, *The multiscale Robin coupled method for flows in porous media*, J. Comput. Phys., 355 (2018), pp. 1–21, https://doi.org/10.1016/j.jcp.2017.11.002.
[23] R. T. Guiraldello, R. F. Ausas, F. S. Sousa, F. Pereira, and G. C. Buscaglia, *Interface spaces for the multiscale Robin coupled method in reservoir simulation*, Math. Comput. Simulation, 164 (2019), pp. 103–119, https://doi.org/10.1016/j.matcom.2018.09.027.
[24] C. Harder, A. L. Madureira, and F. Valentin, *A hybrid-mixed method for elasticity*, ESAIM Math. Model. Numer. Anal., 50 (2016), pp. 311–336, https://doi.org/10.1051/m2an/2015046.
[25] C. Harder, D. Paredes, and F. Valentin, *A family of multiscale hybrid-mixed finite element methods for the Darcy equation with rough coefficients*, J. Comput. Phys., 245 (2013), pp. 107–130, https://doi.org/10.1016/j.jcp.2013.03.019.
[26] C. Harder, D. Paredes, and F. Valentin, *On a multiscale hybrid-mixed method for advective-reactive dominated problems with heterogeneous coefficients*, Multiscale Model. Simul., 13 (2015), pp. 491–518, https://doi.org/10.1137/130938499.
[27] T. J. R. Hughes, G. R. Feijóo, L. Mazzei, and J. B. Quincy, *The variational multiscale method—a paradigm for computational mechanics*, Computer Methods in Applied Mechanics and Engineering, 166 (1998), pp. 3–24.
[28] P.-L. Lions, *On the Schwarz alternating method. III. A variant for nonoverlapping subdomains*, in Third International Symposium on Domain Decomposition Methods for Partial Differential Equations (Houston, TX, 1989), SIAM, Philadelphia, PA, 1990, pp. 202–223.
[29] A. Målqvist and D. Peterseim, *Localization of elliptic multiscale problems*, Math. Comp., 83 (2014), pp. 2583–2603, https://doi.org/10.1090/S0025-5718-2014-02868-8.
[30] A. Målqvist and D. Peterseim, *Numerical homogenization by localized orthogonal decomposition*, vol. 5 of SIAM Spotlights, Society for Industrial and Applied Mathematics (SIAM), Philadelphia, PA, [2021] ©2021.
[31] A. L. Madureira, *Numerical methods and analysis of multiscale problems*, SpringerBriefs in Mathematics, Springer, Cham, 2017, https://doi.org/10.1007/978-3-319-50866-5.
[32] A. L. Madureira and M. Sarkis, *Hybrid localized spectral decomposition for multiscale problems*, SIAM Journal on Numerical Analysis, 59 (2021), pp. 829–863, https://doi.org/10.1137/20M1314896.
[33] S. of Petroleum Engineers, *Spe comparative solution project*, 2000, https://www.spe.org/web/csp/datasets/set02.htm#download (accessed 2000-05-16).
[34] P. Oumaziz, P. Gosselet, K. Saavedra, and N. Tardieu, *Analysis, improvement and limits of the multiscale Latin method*, Comput. Methods Appl. Mech. Engrg., 384 (2021), pp. Paper No. 113955, 26, https://doi.org/10.1016/j.cma.2021.113955.
[35] D. Paredes, F. Valentin, and H. M. Versieux, *Revisiting the robustness of the multiscale hybrid-mixed method: The face-based strategy*, Journal of Computational and Applied Mathematics, 436 (2024), p. 115415, https://doi.org/https://doi.org/10.1016/j.cam.2023.115415.
[36] P.-A. Raviart and J. M. Thomas, *A mixed finite element method for 2nd order elliptic problems*, in Mathematical aspects of finite element methods (Proc. Conf., Consiglio Naz. delle Ricerche (C.N.R.), Rome, 1975), Lecture Notes in Math., Vol. 606, Springer, Berlin, 1977, pp. 292–315.
[37] P.-A. Raviart and J. M. Thomas, *Primal hybrid finite element methods for 2nd order elliptic equations*, Math. Comp., 31 (1977), pp. 391–413, https://doi.org/10.2307/2006423.
[38] F. F. Rocha, F. S. Sousa, R. F. Ausas, G. C. Buscaglia, and F. Pereira, *Multiscale mixed methods for two-phase flows in high-contrast porous media*, J. Comput. Phys., 409 (2020), pp. 109316, 20, https://doi.org/10.1016/j.jcp.2020.109316.
[39] J. Xu and L. Zikatanov, *Some observations on Babuška and Brezzi theories*, Numer. Math., 94 (2003), pp. 195–202, https://doi.org/10.1007/s002110100308.